AD709049

D6-24472

FEBRUARY 1970

EFFECT OF MICROSTRUCTURE ON THE STRENGTH, TOUGHNESS, AND STRESS-CORROSION CRACKING SUSCEPTIBILITY OF A METASTABLE BETA TITANIUM ALLOY (Ti-11.5Mo-6Zr-4.5Sn)

By
JOHN A. FEENEY
MARTIN J. BLACKBURN

DDC
RECEIVED
JUL 24 1970
E

BOEING COMMERCIAL AIRPLANE GROUP
SEATTLE, WASHINGTON

Reproduced by the
CLEARINGHOUSE
for Federal Scientific & Technical
Information Springfield Va. 22151

Sponsored in Part by
Advanced Research Projects Agency
ARPA Order No. 878

This document has been approved for public release and sale; its distribution is unlimited.

79

EFFECT OF MICROSTRUCTURE ON THE STRENGTH, TOUGHNESS, AND STRESS-CORROSION CRACKING SUSCEPTIBILITY OF A METASTABLE BETA TITANIUM ALLOY (Ti-11.5Mo-6Zr-4.5Sn)

J. A. Feeney and M. J. Blackburn

ABSTRACT

This paper describes the influence of microstructure on the mechanical properties of the alloy Ti-11.5Mo-6Zr-4.5Sn. The phase transformations are similar to those that occur in binary Ti-Mo alloys containing 10% to 12% Mo. Thus the β-phase can be retained by quenching from above 1400°F. The β-phase deforms in a complex manner, including mechanical twinning, and is characterized by low strength, high ductility, and high toughness. The ω-phase, which also forms on quenching, is stable at temperatures up to 800°F. Yield strengths of up to 220 ksi have been measured in (β + ω) structures, the strength level being dependent on the size and volume fraction of the ω-phase. In contrast, fracture toughness reaches a minimum value of ~ 20 ksi $\sqrt{\text{in.}}$ when the ω-particle size $\geq$ 100 Å. (β + α) structures show good combinations of yield strength and fracture toughness. Unfortunately, the best combinations are susceptible to stress-corrosion cracking in aqueous solutions containing halide ions.

INTRODUCTION

Transition elements that tend to stabilize the high-temperature equilibrium body-centered cubic β-phase of titanium can be divided into two types: (1) those forming β-isomorphous systems (e.g., Ti-Mo, Ti-V, Ti-Nb) and (2) those forming β-eutectoid systems (e.g., Ti-Cu, Ti-Ni, Ti-Cr).

J. A. Feeney is associated with the Commercial Airplane Group and M. J. Blackburn is associated with the Boeing Scientific Research Laboratory, The Boeing Company, Seattle, Washington.

In the binary Ti-Mo system, the products obtained on quenching from the β-phase field are summarized in Fig. 1 (1-9). Also included are the phases obtained on aging and on plastic deformation of the retained metastable β-phase. It is apparent that the binary Ti-Mo system is quite complex and that small changes in molybdenum content may markedly change the transformation behavior.

The first metastable beta alloy to be produced in commercial quantities, called B120 VCA, had the nominal composition Ti-13V-11Cr-3Al. Although possessing both good room-temperature formability and good heat-treatment response, this alloy was difficult to hot roll and embrittled at service temperatures above 600°F. The embrittlement was attributed to the precipitation of the intermetallic compound $TiCr_2$ (10).

The alloy Ti-11.5Mo-6Zr-4.5Sn, called Beta III, was specifically designed as a "compound free" alloy to circumvent the embrittlement problems experienced with B120 VCA (11,12). Molybdenum is completely isomorphous with beta titanium at high temperatures and is a strong beta stabilizer. Tin strengthens both the α - and β-phases and up to 20% is soluble in both (13); thus the formation of such compounds as Ti_3Sn and Ti_5Sn_3 was considered unlikely in Beta III. Zirconium combats the severe problem of gravity segregation experienced with adding the high-density and high-melting-point element molybdenum directly to the melt. Zirconium, like tin, strengthens both the α - and β-phases.

Work to date on Beta III has been mainly limited to characterizing the alloy's formability, weldability, and engineering properties (11,12). The purpose of the present investigation is to determine the phase transformations that occur in this metastable beta alloy and then relate the contribution of microstructure to the alloy's strength, toughness, and susceptibility to stress-corrosion cracking. A previous paper (14) has described and discussed the deformation characteristics of the metastable β-phase in terms of slip mode, twinning mode, and stress-induced martensite formation.

In general, the transformations and properties of Beta III may be expected to be similar to those found in binary Ti-Mo alloys containing ~12% Mo.

MATERIAL

The Beta III for this study was supplied by the Crucible Steel Corporation; the form and chemical composition of the material are shown in Table 1. Sheet material was used to study phase transformations, and plate and bar stock was used to determine mechanical properties.

EXPERIMENTAL PROCEDURE

Tensile properties and fracture toughness values were determined on a standard Instron machine. Tension specimens 0.25 in. in diameter in the gage length were loaded at a constant strain rate of 0.005 in./in./min. Fatigue precracked notched bend specimens 7 by 1.5 by 0.625 in., together with standard size precracked Charpy specimens, were loaded in three-point bending to determine plane-strain fracture toughness K_{Ic} ; the data were analyzed using the recommended ASTM procedure (15).

Similar notched bend specimens were also used to determine the susceptibility of Beta III to stress-corrosion cracking. Specimens were deadweight loaded in cantilever bending according to the technique described by Brown (16). The environment, 3.5% aqueous NaCl solution, was continually dripped into the specimen notch. Stress intensity was calculated from the equation given by Brown and Srawley (17) by assuming that cantilever bending corresponds to pure bending. The results of the stress-corrosion tests were plotted as initial applied stress intensity K_{Ii} versus time to failure, and the plane-strain threshold stress-intensity level K_{Iscc} , below which crack growth did not occur, was determined. Fatigue precracked single-edge-notched specimens 6 in. long, 1 in. wide, and 0.1 in. thick were used to determine crack velocity characteristics in 0.6 M KCl, saturated KI, and distilled water; the experimental details are described elsewhere (18,19).

All specimens were solution treated above the beta transus, then water quenched. Specimens solution treated 1 hr at 1500°F and at 1600°F had grain sizes of $\bar{L}$ = 0.22 mm and $\bar{L}$ = 0.30 mm, respectively ($\bar{L}$ = mean linear intercept). Aging was carried out in neutral salt baths or in air-circulating furnaces with temperature control to ±10°F.

Hardness tests were performed on a standard Tukon machine, using a 10-kg load and a 16-mm objective.

Phase identification by X-ray analysis was carried out on a Siemens Crystalloflex IV instrument, using a copper tube, a scintillation counter, and a pulse height analyzer to minimize fluorescent radiation.

Germanium-shadowed replicas for fractographic analysis were prepared by the normal two-step technique. Thin foils were prepared by the standard method prescribed for titanium alloys and outlined previously (20).

RESULTS

AS-QUENCHED STRUCTURE

In most as-quenched specimens the ω-phase was detected by both electron and X-ray diffraction techniques, the maximum particle size determined by dark-field imaging being less than 25 Å. Similar observations have been made on other titanium alloys, including Ti-11.6Mo (2).

Binary Ti-Mo alloys containing greater than 11% Mo undergo a stress-induced transformation when deformed (2,6,7,8,9). This transformation results in a high degree of ductility, with over 30% elongation being reported from tension tests conducted at room temperature (21,22).

Beta III exhibits a similar "transformation" when deformed at low temperatures. Some of the characteristics of this "transformation" that influence the ductility, fracture mode, and kinetics of precipitation are briefly described as follows. Between -320°F and +300°F, Beta III deforms primarily by multiple-order mechanical twinning and to a lesser extent by slip and stress-induced orthorhombic martensite formation. Figure 2a shows the morphology of first-order twins after 2% uniform elongation. At this low strain, the twins are straight-sided for a considerable portion of their length and are similar to those reported by Young et al. (23) in Ti-Mn alloys. At intermediate strains (4% to 6% uniform elongation), the twins assume a lenticular shape and contain several variants of internal striations, as shown in Fig. 2b.

Transmission electron microscopy has been used to examine the finer details of this twinning mode. The high dislocation density within first-order twins formed during 1% to 2% uniform elongation is shown in Fig. 3a. Compare this with the multiple-order twins formed after 10% uniform elongation (Fig. 3b).

AGING STUDIES

Aging Below 800°F

At aging temperatures below 800°F, progressive formation of the ω-phase is responsible for strengthening. The variation of hardness with aging time at 700°F, 550°F, and 400°F is shown in Fig. 4. It can be seen that at the lower aging temperatures such as 400°F only a small increase in hardness occurs after an initial incubation period of 120 min. In contrast, at 700°F aging commences without an incubation period, and a large increase in hardness occurs. The ω-phase morphology is ellipsoidal, with a typical aspect ratio of 2.5:1. In binary Ti-Mo alloys, the ω-phase morphology is also ellipsoidal, and particle sizes* up to 3000 Å have been reported (2). In this investigation, the average particle sizes observed in Beta III ranged from 25 Å to 900 Å, depending upon the aging temperature. At the maximum observed hardness levels produced on aging at 550°F and 700°F, particle sizes of 100 Å and 900 Å, respectively, were developed (see Figs. 5a and 5b).

Overaging at 700°F was not associated with the initiation of the $\beta_{rich} + \omega \longrightarrow \beta_{equil} + \omega + \alpha$ reaction. After aging for 1000 hr at 700°F, the ω-phase was the only precipitate present.

Typical selected-area diffraction zones used both for identifying ω-phase and obtaining dark-field micrographs in titanium alloys and zirconium alloys are $[110]_\beta$, $[311]_\beta$, $[210]_\beta$ (2,24,25), and, by tilting about a 110 axis, such zones as $[221]_\beta$ and $[112]_\beta$ (26). A $[110]_\beta$ pattern is shown in Fig. 6a and a second zone $[531]_\beta \parallel [2423]_\omega$, not previously reported, is shown in Fig. 6b. Because of the superposition

*Particle size refers to the maximum dimension along the major axis of the ellipsoids.

of the matrix and ω-phase reflections, the $[100]_\beta$ and $[111]_\beta$ zones cannot be used for ω-phase identification; however, these zones can be used for delineating the nucleation and growth characteristics of α-phase precipitation, since not all α-phase and β-phase reflections are superimposed.

Aging Above 850°F

The hardness versus time curves for aging at 850°F, 1000°F, and 1150°F are shown in Fig. 7. The curves are classical in shape, showing a lower peak hardness at shorter times the higher the aging temperature. Slight overaging is also apparent at each aging temperature. At 1150°F, however, there is a marked increase in hardness at times over 100 hr. This secondary hardening effect far exceeds the initial peak hardness obtained at times between 5 min and 10 min.

At aging temperatures above 850°F, α-phase precipitation is responsible for strengthening. The α-phase morphology is typically Widmanstätten, as shown in Fig. 8, and proceeds from both transgranular nucleation sites and from side plates that emanate from the grain boundaries.

The marked incubation period associated with aging at 850°F (see Fig. 7) offers an area for study of α-phase nucleation. Two zones, the $[110]_\beta$ and $[111]_\beta$, were followed, and the pertinent results are shown in Figs. 9a through 9d. It can be seen that on increasing the aging time from 5 min to 15 min, ω-phase precipitation occurs. The pronounced streaking of the ω-phase reflections shown in Fig. 9b is characteristic of the early stages of ω-phase formation (2). Compare this pattern with that of Fig. 6a, which is typical of specimens containing ω-phase particles > 100 Å in diameter.

As shown in Fig. 9c, no α-phase reflections are apparent after aging 15 min at 850°F. However, in a few isolated areas, elongated arrays of dislocations, possibly interfacial dislocations, were observed during bright-field imaging. On tilting these arrays out of contrast, no visible signs of precipitate could be discerned; therefore, it is possible that such dislocation arrays may be associated with spontaneous

transformation, as discussed below. When the aging time is increased to 2 hr, streaked α-phase reflections are apparent on the $[111]_\beta$ zone, as shown in Fig. 9d, and the microstructure consists of well-developed α-phase plates. Associated with these first-formed plates are interfacial dislocations and dislocations that apparently emanate from the plate interfaces (see Fig. 10). Attempts to analyze the interfacial dislocations by standard $g \cdot b = 0$ techniques were rendered impossible by the interference of spontaneous transformation, which is often encountered in titanium alloys (2,20). A typical example of the problem of interpretation encountered with spontaneous transformation during contrast experiments is shown in Fig. 11.

Aging At 800°F

In the narrow temperature zone 800°F ± 10°F, the α-phase and ω-phase grow simultaneously; that is, the two phases coexist throughout most of the aging cycle. Figure 12 shows the hardness versus time curves for aging at 700°F and 850°F plotted with that for aging at 800°F. It can be seen that the aging characteristics at 800°F are apparently a compromise between those at the two other aging temperatures. For example, it would be expected from classical age-hardening behavior that if α-phase precipitation alone were controlling the aging kinetics (see Fig. 7), the incubation period at 800°F would be much longer than that at 850°F and the aging curve would not exhibit a positive slope in the incubation period.

Thin foil transmission electron microscopy has revealed that the bimodal distribution of α-phase and ω-phase is not uniform from grain to grain and that α-phase is the predominant phase at any stage of the aging cycle at 800°F. Indeed, in some grains the ω-phase could not be unambiguously identified.

The α-phase has an ellipsoidal morphology in the early stages of aging at 800°F that persists to times that produce peak hardness, when the more characteristic needlelike α-phase morphology emerges. The two α-phase morphologies are shown in Figs. 13a and 13b.

As shown earlier (Fig. 5), the ω-phase also has an ellipsoidal morphology in Beta III; thus, during bright-field imaging it is im-

possible to distinguish between the α - and ω-phases. With dark-field imaging, however, region A in Fig. 13c shows the typical particle size and shape of the ω-phase, whereas the size and contrast of the precipitates in region B suggest that some transformation to α-phase has taken place.

Time-temperature-transformation curves that summarize the preceding microstructural and hardness surveys are shown in Fig. 14, together with the T-T-T curves for the binary alloy Ti-13Mo (22,27). It should be noted that the transformation curves for Beta III were generated from quenched and aged specimens and not from specimens quenched directly to an isothermal holding temperature.

Effect of Room-Temperature Prior Deformation

The influence of prior deformation on the subsequent hardening response at aging temperatures 700°F and 1000°F is shown in Figs. 4 and 7, respectively.

At 700°F, the hardness of deformed specimens progressively increases with aging time in a manner similar to that of undeformed specimens. At the commencement of aging, the hardness level for deformed specimens is much greater than for undeformed specimens, but at aging times near peak hardness the two curves tend to merge. The aging time to attain peak hardness at 700°F is slightly reduced by prior deformation.

The formation of the ω-phase at 700°F is only slightly affected by prior deformation. Figure 15a shows matrix precipitation of the ω-phase in a specimen deformed 2% and then aged at 700°F; the deformation twins are out of contrast in this dark-field micrograph. The ω-phase also forms within the deformation twins, as shown in Fig. 15b. At shorter aging times, the particle size of the ω-phase is somewhat smaller within the deformation twins than within the matrix. At aging times that produce peak hardness, however, no significant difference in ω-phase particle size can be discerned. In addition, the ω-phase particle size is the same in both the deformed and undeformed specimens at peak hardness. In contrast to undeformed specimens, the $\beta_{rich} + \omega \longrightarrow \beta_{equil} + \omega + \alpha$ reaction was observed in deformed specimens

slightly overaged at 700°F; therefore this reaction is stimulated by the prior deformation.

As shown in Fig. 7, the hardness of specimens prior deformed at room temperature and aged at 1000°F does not increase with increasing aging time. Indeed, the general trend is to a decreasing hardness, which contrasts with the response of deformed specimens aged at 700°F. Further, although the hardness curves for deformed and undeformed specimens aged at 1000°F merge at the longer aging times, there is still a difference of 35 DPN at peak hardness.

Thin foil examination showed that room-temperature prior deformation stimulated the precipitation of the α-phase in both the matrix and the twins on aging at 1000°F. Both primary and secondary twin interfaces are favored sites for α-phase nucleation at the higher aging temperatures, as may be seen in Fig. 15c.

EFFECT OF MICROSTRUCTURE ON YIELD STRENGTH AND FRACTURE TOUGHNESS

Tension specimens of Beta III in the as-quenched condition had yield strengths of 85 ksi and exhibited uniform elongations up to 35%.

As mentioned, the as-quenched β-phase structure contained ω-phase particles < 25 Å in diameter. Aging at temperatures below 800°F to produce ω-phase particles ≥ 100 Å caused tension specimens to fail in a brittle manner without general yielding. Such failures often originated from faint machine markings in both the gage length and shoulder radius, from extensometer location dimples, and from thread roots located in the loading fixtures. Such brittle specimens were therefore tested in compression and are suitably identified in both Figs. 16a and 16b.*

The dramatic effect of ω-phase precipitation on the yield strength and fracture toughness of Beta III is shown in Figs. 16a and 16b for

*In certain heat-treatment conditions, the fracture toughness values failed to comply with the ASTM validity requirements for K_{Ic}, which require that the specimen thickness $t > 2.5\left(\frac{K}{\sigma_{ys}}\right)^2$, where σ_{ys} = tensile yield stress. Such specimens are identified as K_{IQ} and are included to show general trends.

aging temperatures 550°F and 700°F, respectively. As with hardness, only a small increase in yield strength is obtained on aging at 550°F, even after 500 hr (see Figs. 4 and 16a), at which time the ω-phase has a particle size of 100 Å. There is also a corresponding decrease in fracture toughness from 65.9 ksi $\sqrt{\text{in.}}$ to 19.4 ksi $\sqrt{\text{in.}}$ with increasing aging time at 550°F. Yield strength increases rapidly on aging at 700°F, again in agreement with the hardness results. The maximum yield strength of 220 ksi is associated with an average particle size of 900 Å. In contrast, fracture toughness reaches a limiting value of ~ 20 ksi $\sqrt{\text{in.}}$ early in the aging cycle (Fig. 16b) and is thus apparently independent of both particle size and yield strength when the ω-phase particle size is greater than 100 Å.

A systematic study of the fracture mode of ω-phase-strengthened specimens revealed that in the highest strengthened condition, Beta III does not show all the features of classical cleavage. Indeed, although extremely brittle macroscopically, that is, in terms of K_{Ic} and low-power optical appearance, the fractographic surfaces exhibit most of the characteristics of a microscopically ductile fracture mode. Similar observations were reported by Williams et al. (28) for an ω-phase-strengthened Ti-8Mn alloy. Figures 17a through 17d show that the fracture topology of (β + ω) structures is extremely variable. Figure 17a indicates that such variations are sensitive to grain orientation. The main feature of the fracture topologies is that they all contain dimples. In Fig. 17b the dimples are very shallow and the general fracture appearance is almost cleavagelike. In Figs. 17c and 17d, the dimples are more pronounced, but additional features in Fig. 17d are the intermittent tear ridges. Crack propagation was also studied in a prepolished double cantilever beam specimen (19) and examined with an optical microscope. It was observed that the crack propagated by two distinct modes, each apparently dependent upon grain orientation. In the first type (Fig. 18a), the crack is extremely straight, often propagating without deviation across a single grain, and with little associated plastic deformation. In the second type (Fig. 18b), the crack is more irregular, branching is common, and a higher degree of plastic deformation is observed adjacent to the fracture surfaces.

The effect of the α-phase precipitation on yield strength and fracture toughness of Beta III with aging at 900°F and at 1150°F is shown in Figs. 19a and 19b, respectively. It is apparent that the best combination of strength and toughness is obtained by aging for 32 hr at 900°F, which results in the precipitation of a fine dispersion of α-phase. The low fracture toughness value obtained for specimens aged 30 min at 900°F (Fig. 19a) was very reproducible. This behavior may be explained by the large mass of the fracture toughness specimen, which results in a slow heating and slow cooling rate through the ω-phase transformation region during the aging cycle. Hence the high volume fraction of β-phase may be slightly embrittled by this treatment. In contrast to the sheet material aged at 1150°F, no secondary hardening effect, as measured by yield strength determinations, was achieved in the plate material. Further work is in progress to account for this discrepancy. It is possible that minor changes in chemical composition may explain this behavior; however, it should be noted that the aging times used for plate were somewhat shorter than those used for sheet material.

The predominant fracture mode of α-phase-strengthened Beta III is by microvoid formation. No correlation can be made between dimple size and such factors as aging temperature, aging time at temperature, volume fraction, or plate size of the α-phase, since the dimple size varies considerably from grain to grain. A typical example of the variation in dimple size is shown in Figs. 20a through 20d for a single specimen aged 100 hr at 900°F.

EFFECT OF MICROSTRUCTURE ON STRESS-CORROSION CRACKING SUSCEPTIBILITY

In agreement with work on alloys Ti-8Mn and Ti-11.6Mo (29), as-quenched and ω-phase-strengthened structures in Beta III showed no environmental cracking in halide solutions. However, the ($\beta + \alpha$) microstructures were susceptible to stress-corrosion cracking, as shown in Figs. 21, 22a, and 22b, the degree of susceptibility being strongly dependent on the aging temperature, the environment, and the applied potential.

In Fig. 21 the K_{Ii} versus time to failure in 3.5% NaCl solution is shown for notched bend specimens aged at 900°F and tested under open circuit conditions. These data give a threshold level K_{Iscc} of 26 ksi $\sqrt{in.}$; thus the measure of susceptibility $K_{Iscc}/K_{Ic} = 0.4$. No environmental failures were obtained in similar notched bend specimens aged at 1150°F.

The crack velocity versus K data obtained under controlled potentiostatic conditions are shown in Figs. 22a and 22b for precracked single-edge-notched specimens aged at 900°F and at 1150°F, respectively. The halide solutions (0.6 M KCl and 5.0 M KI) and potentiostatic conditions used in this investigation have been demonstrated to be most severe for Ti-8Al-1Mo-1V (18) and Ti-8Mn (29). Specimens aged at 900°F exhibited a plateau where the crack velocity is independent of stress intensity (Fig. 22a). Similar behavior has also been observed in aluminum alloys and in some titanium alloys (19). In Figs. 22a and 22b, the arrows drawn parallel to the ordinate from the first data points represent the initiation K for environmental growth, which is equivalent to K_{Iscc}. It can be seen in Fig. 22a that the iodide solution promotes a higher crack velocity and a lower K_{Iscc} (or initiation K) than the chloride solution. The K_{Iscc} result for the 0.6 M KCl is also in reasonable agreement with the threshold level determined on similarly aged notched bend specimens in 3.5% NaCl solution with no applied potential. Figure 22a also includes limited crack velocity data for specimens aged at 900°F and tested in distilled water and K_{Ic}/K_{Iscc} values for ω-phase-strengthened specimens aged at 700°F.

Stress-corrosion cracking data for specimens aged at 1150°F and tested under controlled potentiostatic conditions are shown in Fig. 22b. It can be seen, in contrast to the notched bend tests, which were conducted under open circuit conditions, that a marked degree of susceptibility is exhibited. However, variation of crack velocity with stress intensity is different in the two halide solutions. In 0.6 M KCl, the variation of crack velocity with stress intensity is similar to that observed in the specimens aged at 900°F, that is, plateau behavior is exhibited. However, in 5.0 M KI there is no region where crack velocity is independent of K. Furthermore, the initiation stress intensity in

5.0 M KI is significantly affected by strain rate (or crosshead displacement rate). Thus it is not too surprising that no environmental influences were observed in the "static" notched bend tests.

The fracture mode in Beta III in 3.5% NaCl, 0.6 M KCl, and 5.0 M KI is intergranular (Fig. 23). This contrasts with other observations in both α-phase (30) and β-phase (19,29,31) titanium alloys in which stress-corrosion cracking in aqueous solutions has been shown to be associated with a transgranular, cleavage mode of failure. It should also be noted that cracking occurs discontinuously and thus the curves in Figs. 22a and 22b represent average crack velocities.

DISCUSSION

This paper has reported in some detail the microstructural characteristics and mechanical properties of the alloy Ti-11.5Mo-6Zr-4.5Sn (Beta III). We discuss below some of the characteristics that appear to differ from those of similar alloys, e.g., binary Ti-Mo alloys, and attempt to relate some of the mechanical-property results to the microstructural observations.

PHASE TRANSFORMATIONS

Differences in transformation behavior between Beta III and binary Ti-Mo alloys involve (1) the kinetics of formation and the stability range of the ω-phase, (2) the formation of the α-phase from ($\beta + \omega$) structures, and (3) the aging behavior of deformed structures.

Additions of zirconium and tin have little influence on the morphology of the ω-phase, which occurs as ellipsoids in both Beta III and binary Ti-Mo alloys, with the aspect ratio of the ellipsoids being somewhat larger in Beta III. However, the temperature range of stability of the ω-phase is reduced by zirconium and tin, as may be seen by comparing the T-T-T curves for Beta III and Ti-13Mo (Fig. 14). In addition, Williams et al. (32) have shown that the volume fraction of the ω-phase in Beta III is less than in a comparable binary Ti-Mo alloy aged at the same temperature. These factors make direct comparison of particle sizes, particle growth, and hardening rates of Beta III and

Ti-Mo alloys rather difficult. In general, however, the particle sizes are smaller, and hardening rates are slower in Beta III; thus, like aluminum (5), zirconium and tin additions appear to retard ω-phase formation in β-phase alloys.

It has been postulated that the stability and shape of the ω-phase and the formation of the α-phase from $(\beta+\omega)$ structures are related to the mismatch between the β and ω structures (3,5). In systems with a low mismatch and thus with ellipsoidal ω-particle morphology, the α-phase forms by a cellular reaction and at heterogeneous nucleation sites not associated with the ω-phase. In systems with a higher mismatch, in which the ω-phase forms as cuboids (e.g., Ti-V), the α-phase forms at or near the ω-phase particle and grows by consuming the ω-phase. In Beta III, formation of the α-phase may thus be expected to occur heterogeneously. However, the morphology of α-phase after aging at 800°F indicates that the α-phase may form at ω-phase particles, as shown at B in Fig. 13c, so that its formation is more analogous to that in Ti-V than in Ti-Mo alloys. It should be noted, however, that during aging at 800°F the α-phase and ω-phase coexist for long periods and thus the α-phase is not forming from a simple two-phase $(\beta+\omega)$ structure, which may account for this discrepancy. At no stage in the aging of the $(\beta+\omega)$ structures was a cellular reaction observed in Beta III. This may be due to the lower temperature range of stability of the ω-phase, since, in general, cellular growth occurs in binary alloys at higher aging temperatures (2,33).

It is not yet possible to determine whether the effect of prior deformation on the aging characteristics of $(\beta+\omega)$ structures in Beta III is similar to that in Ti-Mo alloys. In binary alloys, prior deformation has been shown to stimulate the nucleation of the α-phase. However, in Beta III, dislocations and twin interfaces do not act as nucleation sites for α-phase formation in the initial stages of aging. This can be seen by comparing Figs. 3a and 15b. Prior deformation does, however, influence the formation of the ω-phase. In the initial stages of aging, particles formed within the twins are smaller than those formed in the matrix, which is probably due to the complete or partial destruction

of the ω-phase by twinning. Thus, renucleation is required in these regions before growth of the ω-phase can occur. The size difference tends to disappear as the aging times are increased. At longer aging times at 700°F, i.e., times longer than 250 hr, α-phase plates are observed adjacent to but not necessarily emanating from twin interfaces. Since deformation twins shrink laterally on removal of the applied stress, it is likely that the highly dislocated, detwinned region stimulates α-phase precipitation. As stated earlier, it is difficult to compare the aging kinetics of Beta III and binary Ti-Mo alloys. For example, aging times of only 14 hr were required to nucleate the α-phase in deformed samples of a Ti-11.6Mo alloy at 750°F (2). The reason for the longer aging times required for Beta III is thus not clear. It is of interest to note, however, that in Ti-11.6Mo (2,21) and Beta III the α-phase is observed in the region of overaging.

MECHANICAL PROPERTIES

It has been shown that the yield strength (and hardness) of Beta III is strongly dependent upon the phase structure. Presently no quantitative analysis of this strength dependence can be given, so the factors discussed below are qualitative and in many cases rather nebulous. The quenched solid solution is very ductile and exhibits mechanical properties similar to those of low interstitial titanium. Such properties are exhibited by several alloys that undergo either martensitic transformations or twinning under the influence of stress (22,23). Aging Beta III to produce the ω-phase results in large increases in strength, which are unfortunately accompanied by drastic reductions in toughness. The aging response at 700°F, which shows that overaging occurs in fully ($\beta + \omega$) structures, indicates that the size, spacing, and volume fraction of the ω-phase influence the flow properties. The maximum strength of 220 ksi is associated with an <u>average</u> particle size of 900 Å. In a recent review of ω-phase formation, Hickman (5) indicated that the mechanism of hardening and embrittlement is not understood. Unfortunately, the present investigation has not provided any great insight into this mechanism, but consideration of the following points may be worthwhile.

1. The nature of dislocation-particle interaction is unknown, i.e., whether particles are sheared or bypassed by dislocations. Electron

microscopy analysis has not proved capable of answering the question, and optical examination of slip lines in deformed or fractured specimens yields ambiguous results. In some cases long, straight slip lines are observed, as at A in Fig. 18c, but in others a wavy and branched slip morphology is found, as at B in Fig. 18c. However, in most cases the slip line heights are large, indicating that strain is concentrated in rather narrow regions.

2. The mechanical properties of the ω-phase are not known, although single ω-phase structures have been produced by hydrostatic pressure.
3. The quantitative analyses of hardening developed for conventional precipitation-hardening systems are probably not applicable, since the volume fraction of the ω-phase is usually ≥ 0.5.
4. There may be an analogy between the hardening processes in ($\beta + \omega$) structures and those in spinodally decomposed alloys. Carpenter (33) has observed rather similar changes in mechanical properties in the Au-Pt system. Although the yield strength is increased in that system, the work-hardening rate and the strain to failure show the most dramatic changes: in the model of work hardening developed for spinodally decomposed alloys, the stress increase due to work hardening is inversely proportional to the sine of the wavelength of the composition fluctuations. If applicable, such a model would predict that overaging would be observed in ($\beta + \omega$) structures, especially if measured by a hardness test that measures both the yield strength and work-hardening properties of a material.

Work is in progress to evaluate in more detail the effect of ω-phase formation on flow stress and work-hardening characteristics of titanium alloys.

The ($\beta + \alpha$) structures show intermediate yield strengths, ductility, and fracture toughness. The effects of the α-phase precipitation on yield strength and fracture toughness (Figs. 19a and 19b) indicate that these properties are influenced by the size, spacing, and volume fraction of the α-phase. It would be expected that the α-phase would be relatively soft, since it contains little molybdenum; thus the composition of the β-phase probably exerts a strong influence on the yield

strength characteristics. In binary Ti-Mo alloys, the flow strength of the β-phase increases by $\simeq$ 70% between 12% and 24% Mo. In these and many titanium alloys, the precipitated phase is softer than the matrix (when considered separately), and strengthening in such systems is not well understood.

FRACTURE TOUGHNESS AND FRACTURE

Beta III in all heat treatments exhibits fracture topologies containing dimples, features that are generally assumed to result from a fracture process involving the formation and growth of voids. Fracture of the (β + α) and β-phase (quenched) structures probably occurs by such a mechanism and the average dimple size is roughly related to fracture toughness. In general, the higher the fracture toughness the larger the dimple size, but quantitative correlations are impossible, as indicated by Fig. 20.

The most interesting fractures observed are those found in (β + ω) structures. Fracture toughness results for specimens aged at 700° and 550°F show that K_{Ic} is independent of ω-particle size when this exceeds $\sim$ 100 Å. Macroscopically, fracture of these (β + ω) structures resembles cleavage-type failures observed in other bcc systems. However, replicated surfaces exhibit small dimples, which are normally characteristic of a more ductile fracture mode. Similar observations have been made on Ti-Mo and Ti-Mn alloys (28). Figures 18a and 18b show that two types of fracture are observed macroscopically—straight and relatively flat cleavagelike cracks associated with little or no observable plastic flow (18a), and branched and serrated cracks associated with a higher plastic strain (18b). Limited single crystal analysis has shown that cracks in these structures run parallel to the $\{100\}_\beta$ planes but with some deviation, so that in many ways the fracture surface resembles a conchoidal fracture. The single crystal results also indicate that the fine dimpled topography shown in Fig. 17c can be correlated with the flat cleavagelike cracks shown in Fig. 18a, whereas the intermittent tear ridges shown in Fig. 17d are probably associated with the irregular crack morphology shown in Fig. 18b. Thus, there would seem to be two possible explanations of the fracture topology of (β + ω) structures.

First, the dimples represent small microvoids, which implies that a strain-controlled failure occurs. The obvious sites for microvoids formation are the $\beta : \omega$ interfaces, which in turn implies that the ω-phase acts as a hard, impenetrable barrier. Unfortunately, there appears to be no correlation of dimple size with ω-particle size. Second, the fracture could be similar to the failure mode observed in some plastics, e.g., polymethyl methacrylate (34). In this case, the dimples would represent the intersection of the primary crack with microcracks formed in advance of the primary crack front. The tear-ridged structure would then represent the momentary arrest lines or striae observed in fractured polymers.

STRESS-CORROSION CRACKING

Ti-7Al-2Cb-1Ta was the first titanium alloy shown to be susceptible to stress-corrosion cracking (SCC) in neutral aqueous solutions (16). Subsequently, it has been found that many titanium alloys exhibit SCC susceptibility in a variety of environments. When added to titanium alloys, molybdenum is considered to reduce SCC susceptibility and tests on binary Ti-Mo alloys have shown that the quenched (β), slow cooled (coarse $\alpha + \beta$), and quenched and aged ($\beta + \omega$) structures are immune to SCC. Thus the observation that Beta III is susceptible to SCC came as a surprise. Much further work is needed to establish the influence of all possible parameters on the SCC susceptibility of Beta III, but some of the characteristics of SCC in this and other Ti alloys are listed below.

1. Cracking is predominantly intergranular in Beta III, whereas it is predominantly transgranular in all other Ti alloys thus far tested in aqueous solutions.
2. Cracking is obviously discontinuous in Beta III; this may also be true of the transgranular SCC in other Ti alloys, but is not obviously so.
3. The halide ions Cl^-, Br^-, and I^- accelerate intergranular cracking in Beta III with respect to that observed in distilled water; they also accelerate transgranular cracking in other Ti alloys.

The effect of heat treatment on SCC susceptibility has not been studied in detail, but it appears that higher aging temperatures result in less susceptible conditions, e.g., compare the results for aging at 900°F and at 1150°F, Figs. 22a and 22b, respectively. By changing the aging temperature, two microstructural factors are changed—the volume fraction and dispersion of the α-phase and the composition of the β-phase. In similar structures in Ti-8Mn, it has been shown that the β-phase composition is the critical factor (19). To gain some insight into the controlling microstructural feature, specimens of a Ti-11.6Mo alloy were aged at 900°F to produce similar (β + α) microstructures. These were then tested in 5.0 M KI at 0 mV and it was found that some intergranular separation occurred. However, the extent of the SCC was limited and the load level for crack propagation was near the fracture load in air. Thus it is concluded that binary Ti-Mo alloys are much less susceptible than Beta III to SCC. It is possible that the additions of tin and zirconium result in the higher degree of SCC susceptibility in Beta III. Further, it is possible that the α-phase is responsible for the susceptibility—this phase occurs as an almost continuous grain boundary film after heat treatment at 900°F. Thus it may be postulated that this film of α-phase, enriched in zirconium and/or tin, renders the alloy susceptible to SCC in halide-containing solutions.

PRACTICAL NOTE

The excellent formability of Beta III in the solution-treated or solution-treated-and-aged condition has resulted in its wide use for aerospace fastener applications (12). In comparison with Ti-6Al-4V, Beta III exhibits good cold headability so that rivets of this material can be installed by conventional gun-driven techniques with the tooling normally employed for aluminum fasteners. Care must be taken, however, in selecting the heat treatment for the fastener, since the precipitation of the ω-phase would cause severe degradation of fracture toughness over long exposure times. It is fortunate that the aging treatment which produces the best combination of cold headability and shear strength in the solution-treated-and-aged condition (e.g., 1100°F for 8 hr) also re-

sults in a greater resistance to SCC. However, if lower aging temperatures are used to produce greater strengths, care should be taken that the components do not come in contact with halide-containing solutions.

CONCLUSIONS

1. The phase transformations that occur in Beta III are similar to those that occur in binary Ti-Mo alloys with approximately the same molybdenum content. Some differences in transformation behavior are observed, however, such as the temperature range of stability of the ω-phase and the aging characteristics of deformed material.

2. In the temperature range -320° to +300°F, the primary deformation mode of Beta III is by mechanical twinning; to a lesser extent, deformation occurs by slip and stress-induced orthorhombic martensite formation.

3. At room temperature, as-quenched structures have a low yield stress, a high ductility, and a high toughness.

4. (β + ω) structures are hard and brittle. At aging temperatures approaching the upper limit of stability of the ω-phase (e.g., 700°F), hardness and yield strength progressively increase with increasing aging time (and increasing particle size of the ω-phase) to maximums of 475 DPN and 220 ksi, respectively. The fracture toughness of (β + ω) structures, however, reaches a minimum value of 22 ksi $\sqrt{\text{in.}}$ when the particle size of the ω-phase exceeds 100 Å, irrespective of aging temperature, aging time, or yield strength.

5. The cracking plane of (β + ω) structures is near $\{100\}_\beta$ and the fracture mode macroscopically resembles cleavage. Microscopically, however, the dimpled fracture topography is more characteristic of a ductile mode of failure.

6. (β + α) structures show good combinations of yield strength and fracture toughness. Unfortunately, the best combinations also exhibit the greatest susceptibility to stress-corrosion cracking in

aqueous solutions containing Cl^- and I^- ions. Higher aging temperatures result in less susceptible conditions in terms of crack velocity or K_{Iscc}/K_{Ic} ratio.

7. In contrast to the stress-corrosion cracking in other titanium alloys, the fracture mode of α-phase-strengthened Ti-11.5Mo-6Zr-4.5Sn in aqueous solutions is intergranular.

8. As-quenched and ($\beta + \omega$) structures are immune to stress-corrosion cracking.

ACKNOWLEDGMENTS

The authors gratefully acknowledge the experimental assistance of R. Lee, A. Raisanan, G. Rassmussen, D. Farwick, A. Ross, and T. Kane. The research was supported in part (JAF) by the Advanced Research Projects Agency of the Department of Defense, ARPA Order No. 878, under Contract No. N00014-66-C0365.

REFERENCES

1. Iu. A. Bagariatskii, G. I. Nosova and T. V. Tagunova, "Factors in the Formation of Metastable Phases in Titanium-Base Alloys," Soviet Phys.-Doklady, Vol. 3, 1959, p. 1014.

2. M. J. Blackburn and J. C. Williams, "Phase Transformations in Ti-Mo and Ti-V Alloys," Trans. AIME, Vol. 242, 1968, p. 2461.

3. J. C. Williams and M. J. Blackburn, "The Influence of Misfit on the Morphology and Stability of the Omega Phase in Ti-Transition Metal Alloys," Trans. AIME, Vol. 245, 1969, p. 2352.

4. B. S. Hickman, "Omega Phase Precipitation in Alloys of Titanium with Transition Metals," Trans. AIME, Vol. 245, 1969, p. 1329.

5. B. S. Hickman, "The Formation of Omega Phase in Titanium and Zirconium Alloys: A Review," Journal of Materials Science, Vol. 4, 1969, p. 554.

6. Y. C. Lui, "Martensitic Transformation in Binary Titanium Alloys," Trans. AIME, Vol. 206, 1956, p. 1036.

7. S. Weinig and E. S. Machlin, "Data for One of the Martensitic Transformations in an 11 Pct Mo-Ti Alloy," Trans. AIME, Vol. 200, 1954, p. 1280.

8. P. Gaunt and J. W. Christian, "The Crystallography of the Transformation in Zirconium and in Two Titanium-Molybdenum Alloys," Acta Met., Vol. 7, 1959, p. 534.

9. R. H. Hiltz, Jr., "Stress Induced Martensitic Transformation of Beta Titanium," Trans. AIME, Vol. 215, 1959, p. 138.

10. V. C. Peterson, H. B. Bomberger and M. B. Vordahl, "An Age Hardening Titanium Alloy," Metal Progress, Vol. 76, 1959, p. 119.

11. V. C. Peterson, J. B. Guernsey and H. A. Johnson, "Properties and Applications of Beta III Titanium," presented at Fifth Annual Meeting of AIAA (Paper No. 68-976), Philadelphia, Pa., October 1968.

12. J. B. Guernsey, V. C. Peterson and E. J. Dulis, "Beta III Titanium Features Cold Formability," Metal Progress, Vol. 96, 1969, p. 121.

13. M. Hansen, Constitution of Binary Alloys, 2nd ed., McGraw-Hill Book Company Inc., New York, 1958.

14. M. J. Blackburn and J. A. Feeney, Stress-Induced Transformations in Ti-Mo Alloys, D6-25210, The Boeing Company, February 1970.

15. "Proposed Recommended Practice for Plane Strain Fracture Toughness Testing of High Strength Metallic Materials Using a Fatigue Cracked Bend Specimen," ASTM Standards, Vol. 31, 1966, p. 1018.

16. B. F. Brown, "A New Stress Corrosion Cracking Test for High Strength Alloys," ASTM Materials Research and Standards, Vol. 6, 1966, p. 129.

17. W. F. Brown, Jr., and J. E. Srawley, Plane Strain Crack Toughness Testing of High Strength Metallic Materials, ASTM STP 410, ASTM, Philadelphia, Pa., 1966.

18. T. R. Beck and M. J. Blackburn, "Stress Corrosion Cracking of Titanium Alloys," J. AIAA, Vol. 6, 1968, p. 326.

19. T. R. Beck, M. J. Blackburn, and M. O. Speidel, Stress Corrosion Cracking of Titanium Alloys: SCC of Aluminum Alloys, Polarization of Titanium Alloys in HCl and Correlation of Titanium and Aluminum SCC Behavior, Quarterly Progress Report No. 11, Contract NAS 7-489, March 1969.

20. M. J. Blackburn and J. C. Williams, "The Preparation of Thin Foils of Titanium Alloys," Trans. AIME, Vol. 239, 1967, p. 287.

21. F. C. Holden, H. R. Ogden, and R. I. Jaffee, "Heat Treatment and Mechanical Properties of Titanium-Molybdenum Alloys," J. Metals, Vol. 8, 1956, p. 1388.

22. R. I. Jaffee, "The Physical Metallurgy of Titanium Alloys," Progr. Metal Phys., Vol. 7, 1958, p. 65.

23. A. P. Young, R. I. Jaffee, and C. M. Schwartz, "Electron Microscope Examination of Deformation in Alpha-Beta Ti-Mn Alloys," Acta Met., Vol. 11, 1963, p. 1097.

24. J. C. Williams and M. J. Blackburn, "A Comparison of Phase Transformations in Three Commercial Titanium Alloys," Trans. Am. Soc. Metals, Vol. 60, 1967, p. 373.

25. W. Bramner and C. G. Rhodes, "Determination of Omega Phase Morphology in Ti-35%Nb by Transmission Electron Microscopy," Phil. Mag., Vol. 16, 1967, p. 477.

26. S. L. Sass, "The Omega Phase in a Zr-25 Atomic % Alloy," Acta Met., Vol. 17, 1969, p. 813.

27. S. A. Spachner and W. Rostoker, Structural Changes of Commercial Titanium and Titanium-Base Alloys on Heat-Treatment, WADC Technical Report 55-352, June 1956.

28. J. C. Williams, R. R. Boyer, and M. J. Blackburn, The Influence of Microstructure on the Fracture Topography of Titanium Alloys, ASTM STP 453, ASTM, Philadelphia, Pa., 1969, p. 215.

29. T. R. Beck and M. J. Blackburn, Stress Corrosion Cracking of Titanium Alloys: SCC of Titanium-8% Mn Alloy, Pitting Corrosion

of Aluminum and Mass-Transport-Kinetics Model for SCC of Titanium, Quarterly Progress Report No. 7, Contract NAS 7-489, March 1968.

30. Proceedings of Conference, Fundamental Aspects of Stress Corrosion Cracking, Ohio State University, edited by R. W. Staehle, NACE, 1969.

31. D. N. Fager and W. F. Spurr, "Some Characteristics of Aqueous Stress Corrosion in Titanium Alloys," Trans. Am. Soc. Metals, Vol. 61, 1968, p. 283.

32. J. C. Williams, H. L. Marcus, and B. S. Hickman, "Effect of Omega Phase on Mechanical Properties of Titanium Alloys," paper presented at Spring Meeting of Metallurgical Society of AIME, Pittsburgh, Pa., 1969.

33. R. W. Carpenter, "Deformation and Fracture of Gold-Platinum Polycrystals Strengthened by Spinodal Decomposition," Acta Met., Vol. 15, 1967, p. 1297.

34. I. Wolcock, J. A. Kies, and S. B. Newman, "Fracture Phenomena in Polymers," Fracture, edited by B. L. Averbach et al., J. Wiley & Sons Inc., New York, 1959.

Table 1 Form and Chemical Composition of Ti-11.5Mo-6Zr-4.5Sn (Beta III)

Form	Chemical Composition						
	Mo (wt%)	Zr (wt%)	Sn (wt%)	Fe (wt%)	H (ppm)	O (ppm)	N (ppm)
Sheet (0.1 in. thick)	11.13	4.83	5.07	0.04	61	1700	94
Plate (0.640 in. thick)	10.71	4.12	4.60	0.03	59	1350	102
Bar (0.5 in. dia)	10.70	5.17	4.88	0.02	53	1670	112

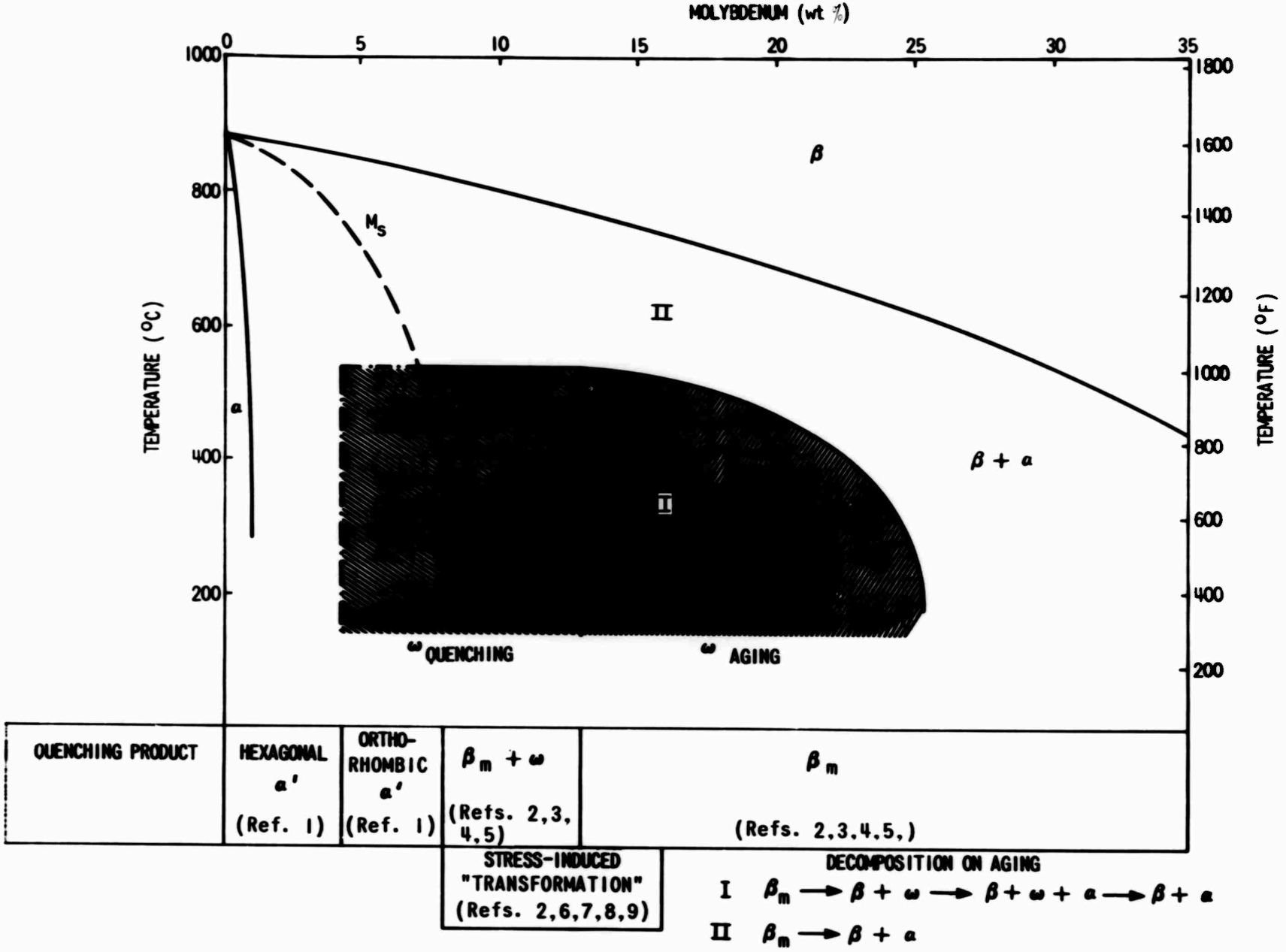

Figure 1 Summary of phase transformations occurring in Ti-Mo alloys in the range 0 wt % to 35 wt % Mo (α'= martensite, β_m = metastable β-phase, ω = ω-phase, M_s = martensite start temperature).

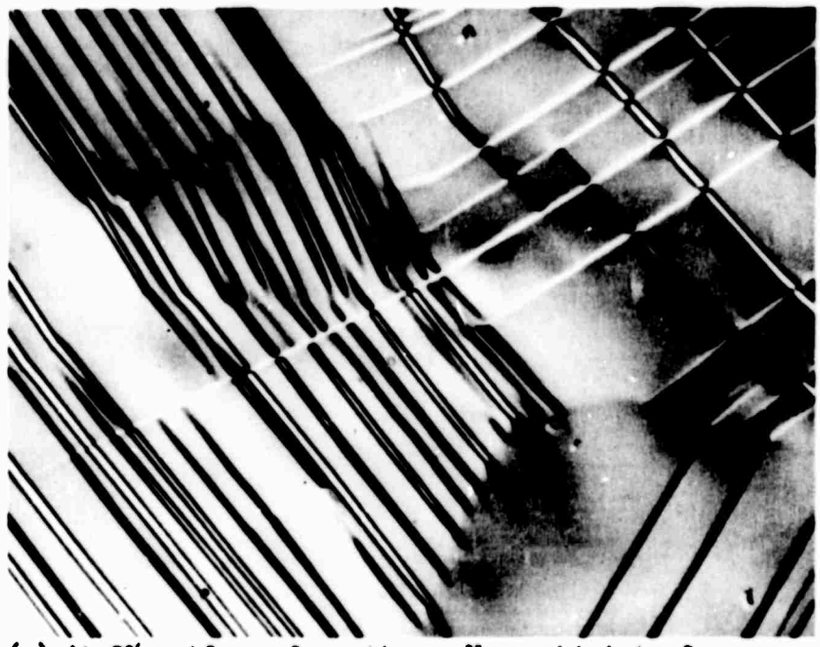

(a) At 2% uniform elongation. Nomarski interference contrast (X750).

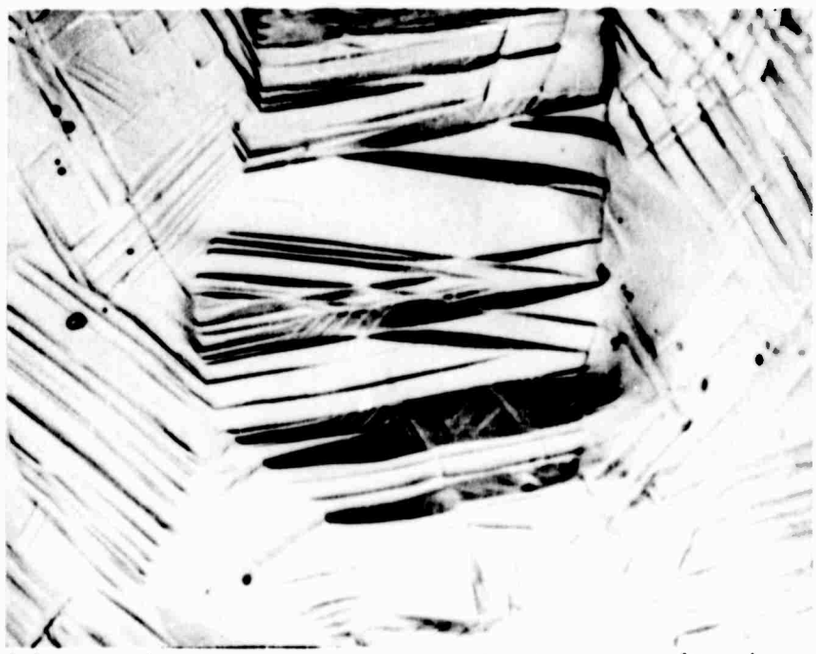

(b) At 10% uniform elongation. Bright field (X750).

Figure 2 Optical micrographs showing deformation twins formed in Beta III at low and intermediate strains.

(a) At 2% uniform elongation. Zone normal ~ $\langle 111 \rangle_\beta$
$g = (0\bar{1}1)_T$. Dark field.

(b) At 10% uniform elongation. Zone normal = $[111]_\beta$.
Bright field.

Figure 3 Electron micrographs showing deformation twins formed in Beta III at low and intermediate strains.

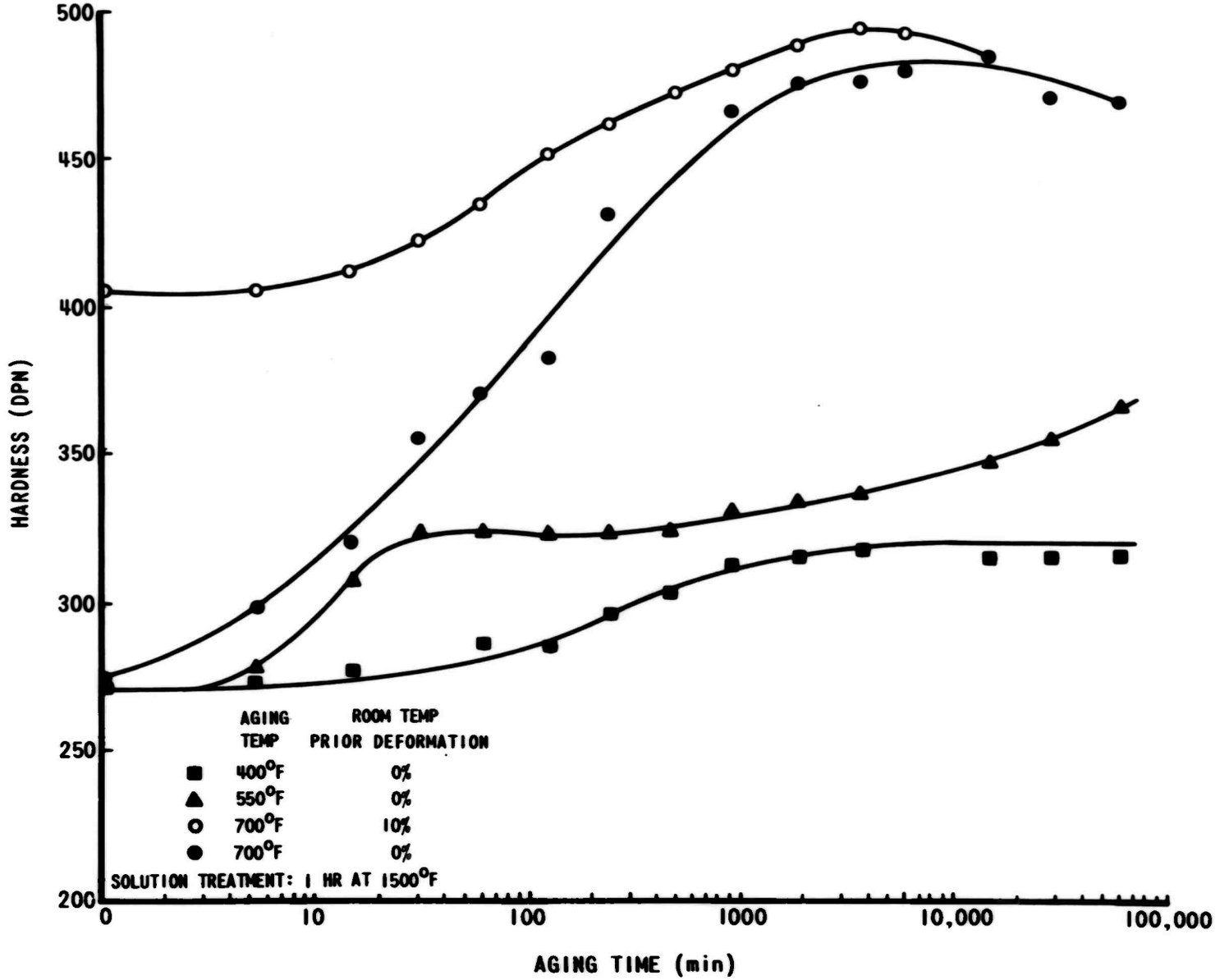

Figure 4 Variation of hardness with aging time for specimens of Beta III aged at 700°F, 550°F, and 400°F.

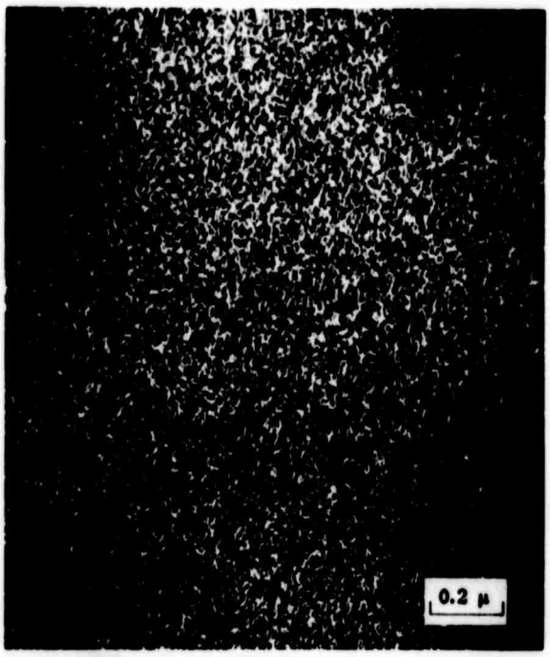

(a) After 1,000 hr at 550°F. Zone normal = $[311]_\beta$
$g = (10\bar{1}1)_\omega$.

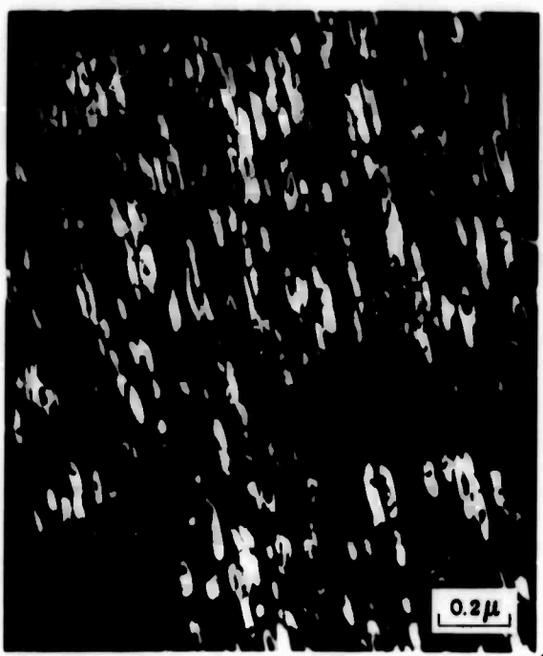

(b) After 500 hr at 700°F. Zone normal = $[110]_\beta$
$g = (0001)_\omega$.

Figure 5 Dark-field electron micrographs showing ω-phase morphology in Beta III at two aging temperatures.

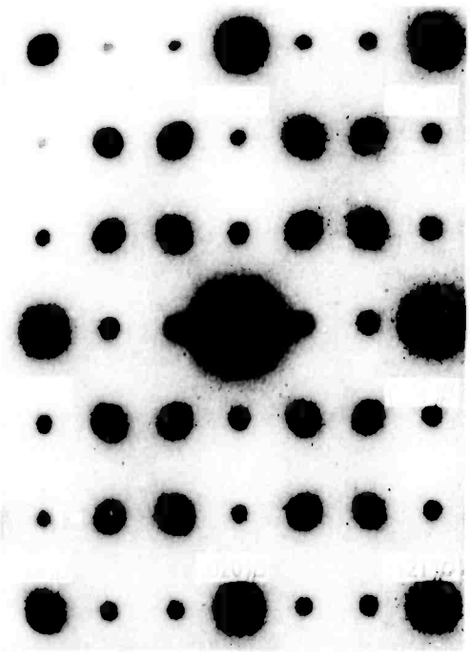

(a) Consists of $[101]_\beta$ zone normal and three ω variants (one $[10\bar{1}4]_\omega$ and two $\langle\bar{1}2\bar{1}0\rangle_\omega$). Detailed indexing of this pattern is given in Ref. 2.

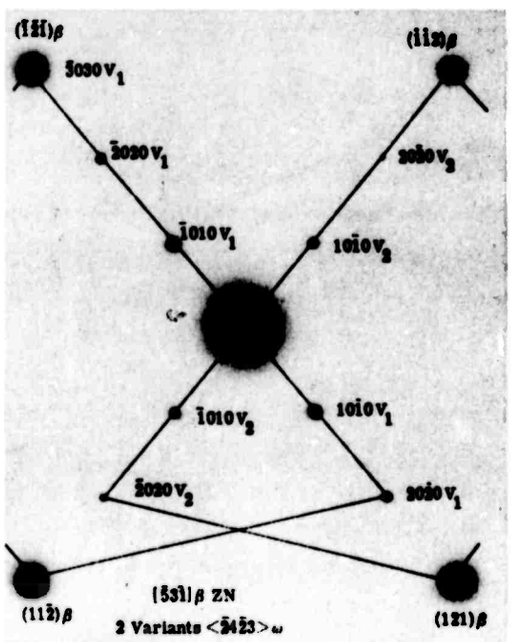

(b) Consists of $[53\bar{1}]_\beta$ zone normal and two variants with $\langle\bar{2}4\bar{2}3\rangle_\omega$ zone normals.

Figure 6 Selected-area diffraction patterns from $(\beta + \omega)$ structures in Beta III.

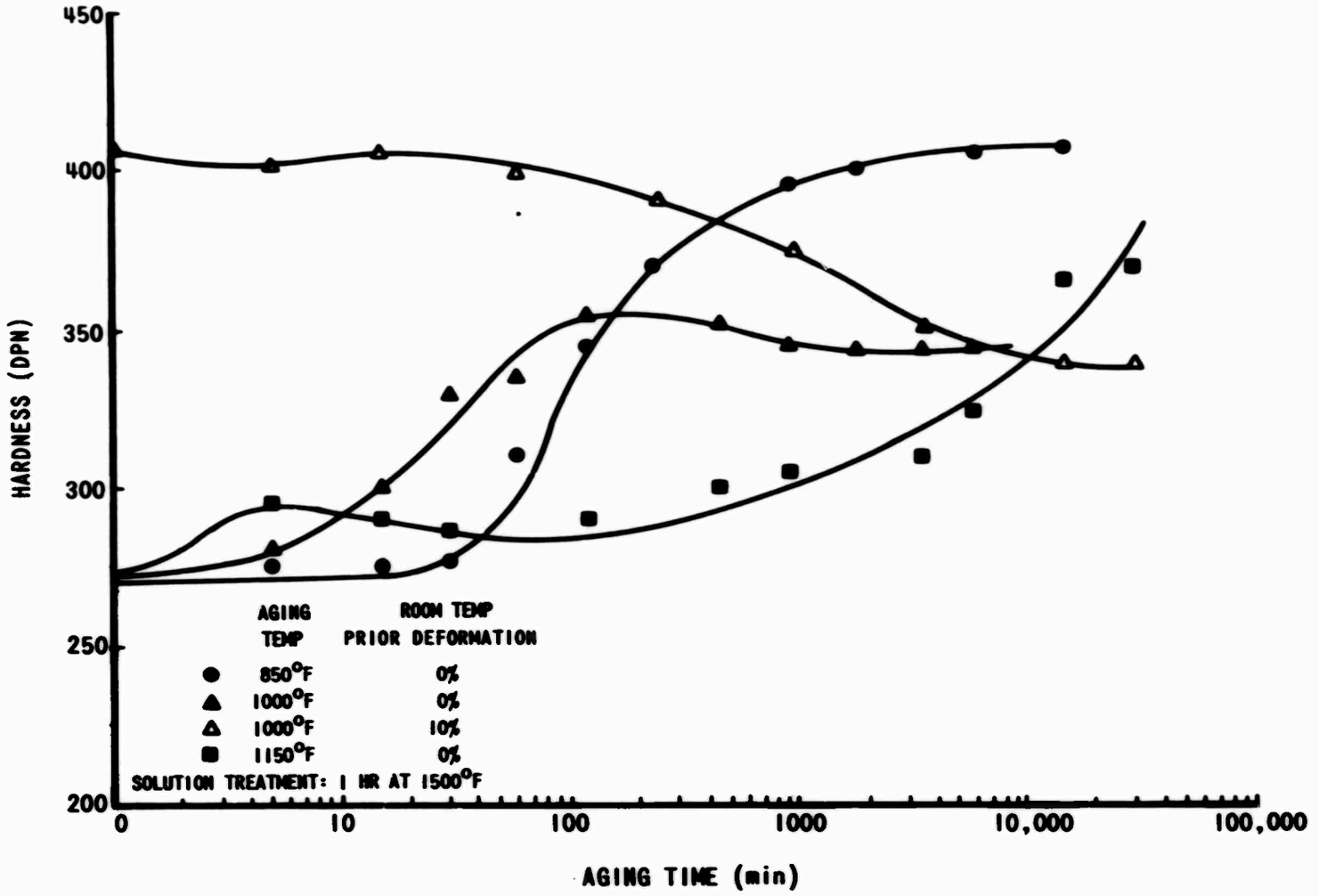

Figure 7 Variation of hardness with aging time for specimens of Beta III aged at 850°F, 1000°F, and 1150°F.

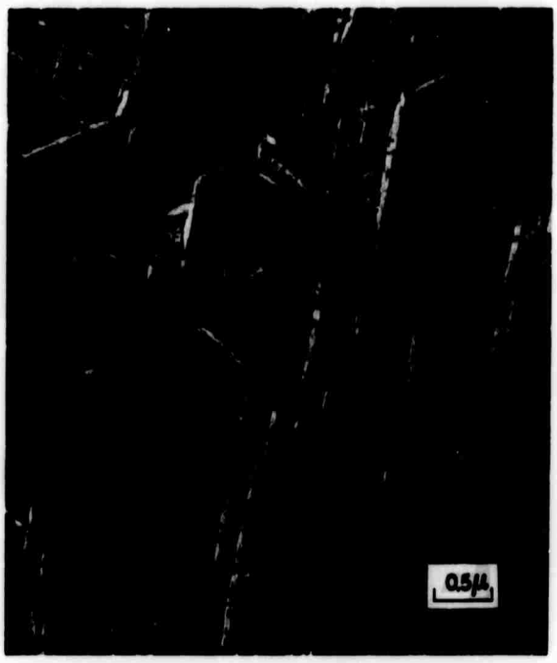

Figure 8 Bright-field electron micrograph of Widmanstätten α-phase formed in Beta III aged 64 hr at 850°F. Zone normal ≃ $\langle 111 \rangle_\beta$.

BLANK PAGE

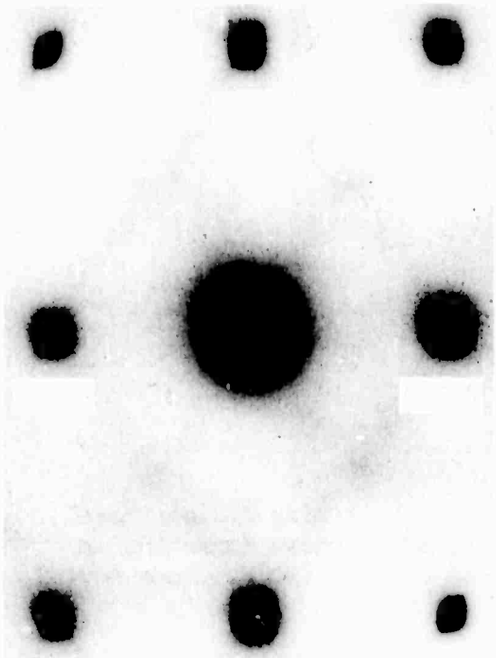

(a) Aged 5 min. $[110]_\beta$ zone normal.

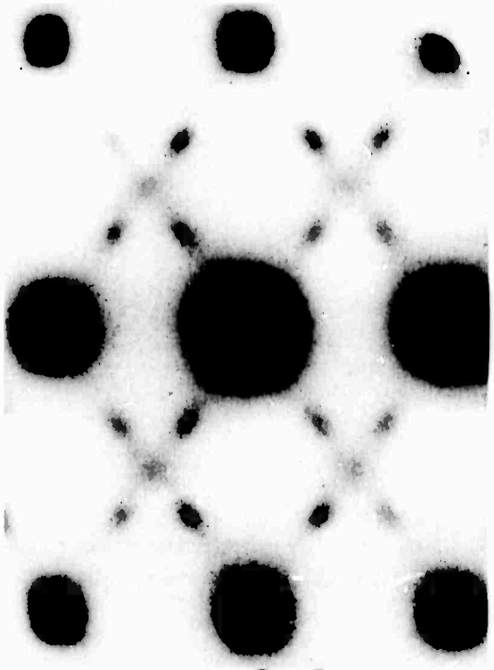

(b) Aged 15 min. $[110]_\beta$ zone normal. Note appearance and pronounced streaking of ω-phase reflections.

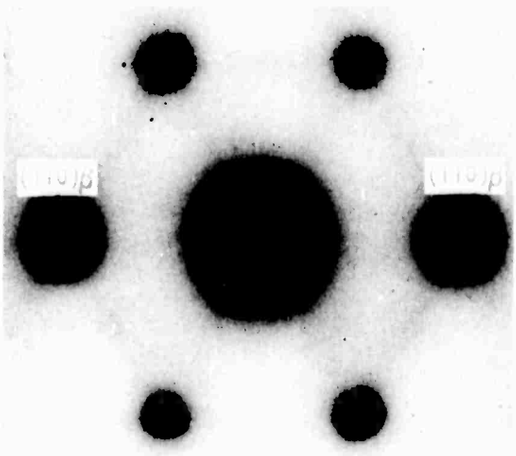

(c) Aged 15 min. $[111]_\beta$ zone normal.

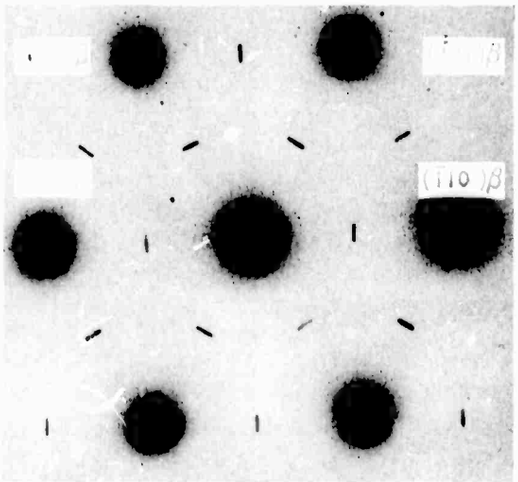

(d) Aged 2 hr. $[111]_\beta$ zone normal. Note appearance of faint α-phase reflections.

Figure 9 Series of selected-area diffraction patterns taken from specimens of Beta III aged at 850°F for various times.

Figure 10 Bright-field electron micrograph showing dislocations associated with early stages of α-phase formation in Beta III. Specimen was aged 2 hr at 850°F. Zone normal $\simeq \langle 311 \rangle_\beta$.

Figure 11 Bright-field electron micrograph illustrating the problems of interpretation encountered with spontaneous transformation during contrast experiments in titanium alloys. Specimen was aged 2 hr at 850°F. Zone normal $\simeq \langle 111 \rangle_\beta$.

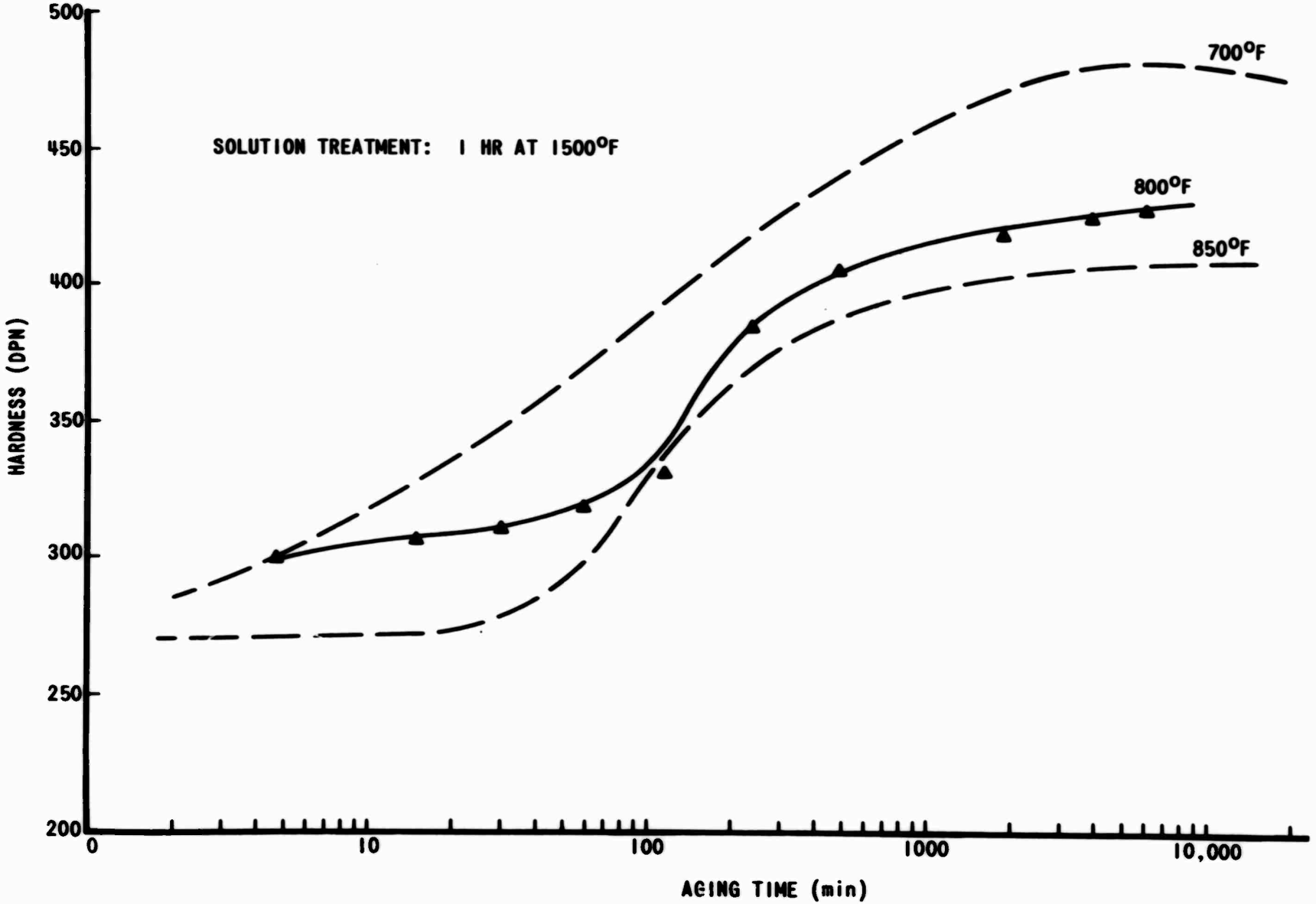

Figure 12 Variation of hardness with aging time for specimens of Beta III aged at 800°F. Hardness curves for specimens aged at 700°F and at 850°F are included for comparison.

(a) Ellipsoidal α-phase (+ ω-phase?). Zone normal = $\langle 111 \rangle_\beta$. Bright field.

(b) Needlelike α-phase. Zone normal = $\langle 111 \rangle_\beta$. Bright field.

(c) ω-phase particles at A and possible transformation of ω-phase particles to α-phase at B. Zone normal = $\langle 110 \rangle_\beta$ g = $(0001)_\omega$. Dark field.

Figure 13 Electron micrographs showing morphology of α-phase and of ω-phase in specimens of Beta III aged 100 hr at 800°F.

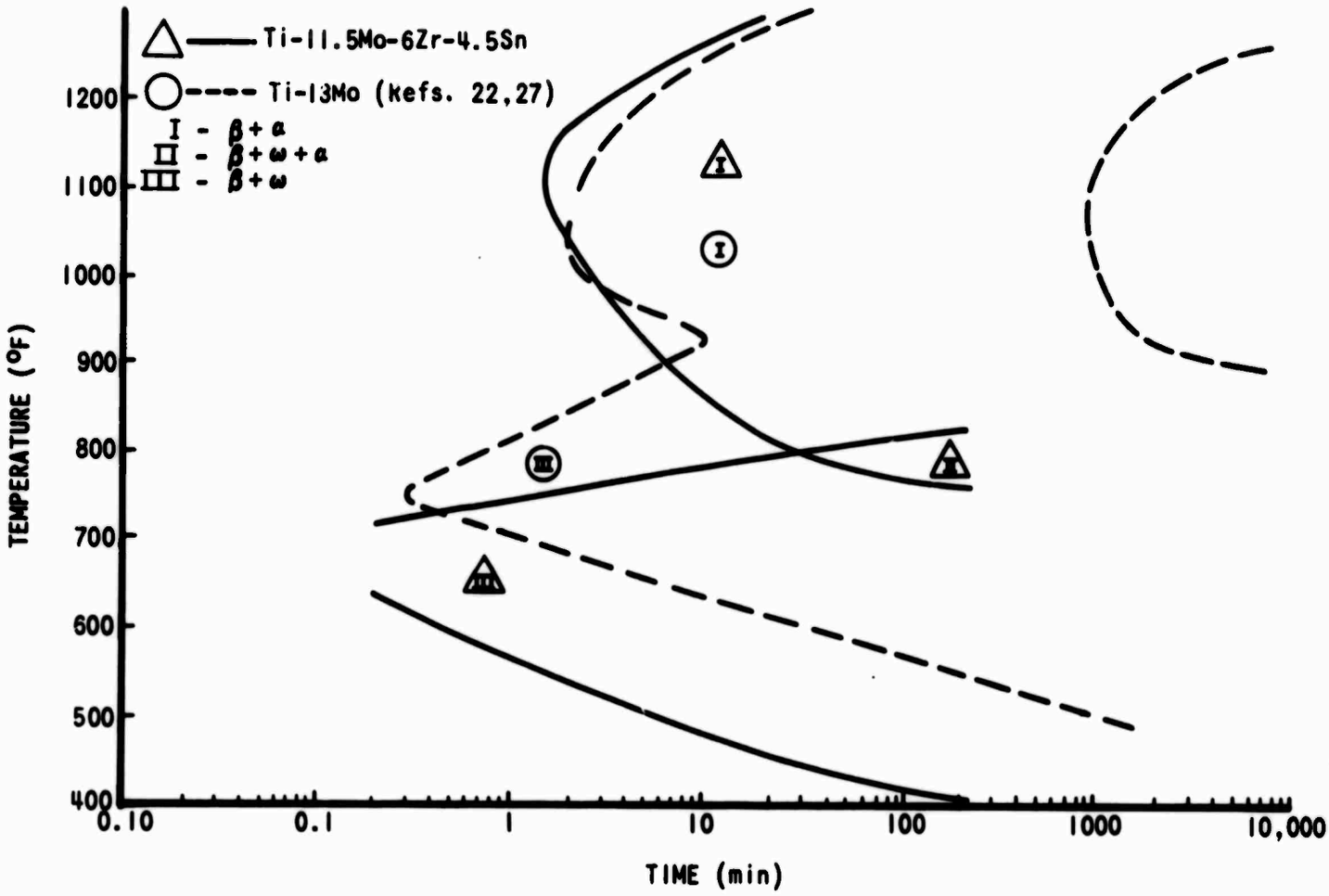

Figure 14 Time-temperature-transformation curves for Beta III and for Ti-13Mo.

(a) Matrix precipitation of the ω-phase in a specimen deformed 2% then aged 15 min at 700°F. Zone normal = $\langle 210 \rangle_\beta$ $g = (2\bar{1}\bar{1}\bar{1})_\omega$. Dark field.

(b) ω-phase particles within a deformation twin in a specimen deformed 2% then aged 30 min at 700°F. Zone normal = $\langle 110 \rangle_\beta$ $g = (0001)_\omega$. Dark field.

(c) α-phase precipitation on first-order and second-order twin interface. Specimen was deformed 5% then aged 250 hr at 1150°F. Zone normal $\simeq \langle 311 \rangle_\beta$. Bright field.

Figure 15 Electron micrographs showing the effect of room-temperature prior deformation on the phase transformations in Beta III.

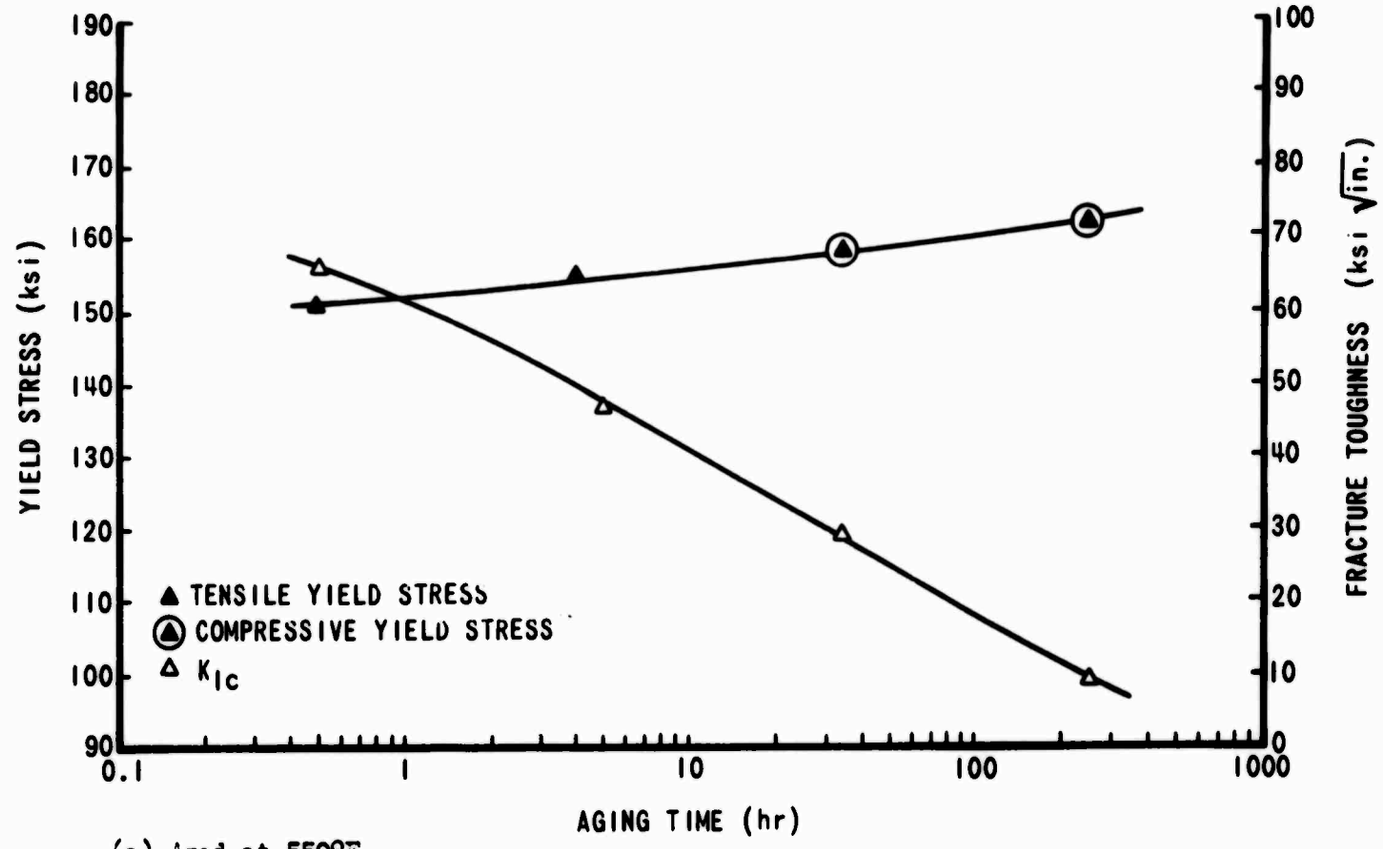

(a) Aged at 550°F.

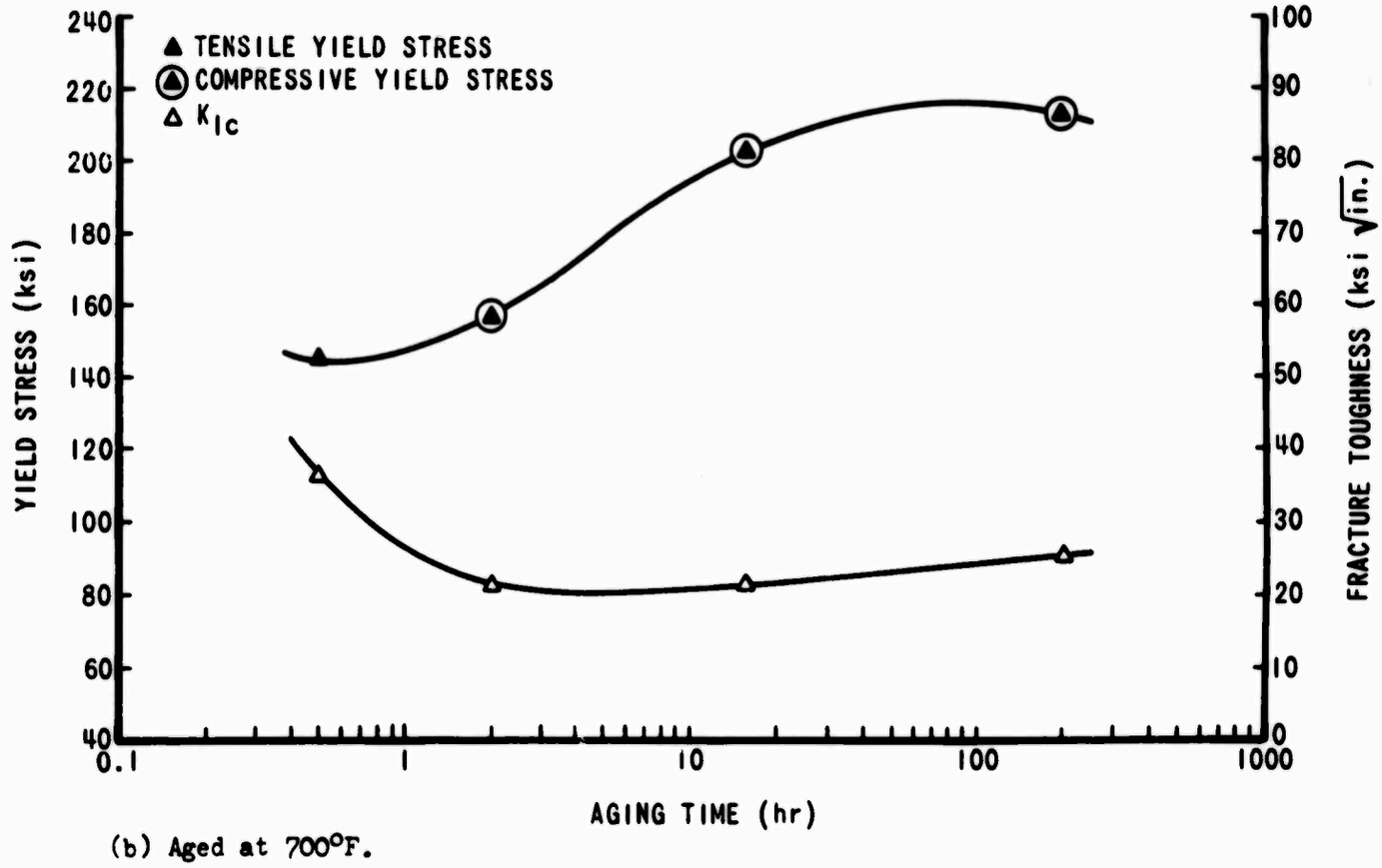

(b) Aged at 700°F.

Figure 16 Effect of ω-phase precipitation on yield strength σ_{ys} and fracture toughness K_{Ic} of Beta III.

(a) Aged 30 min.

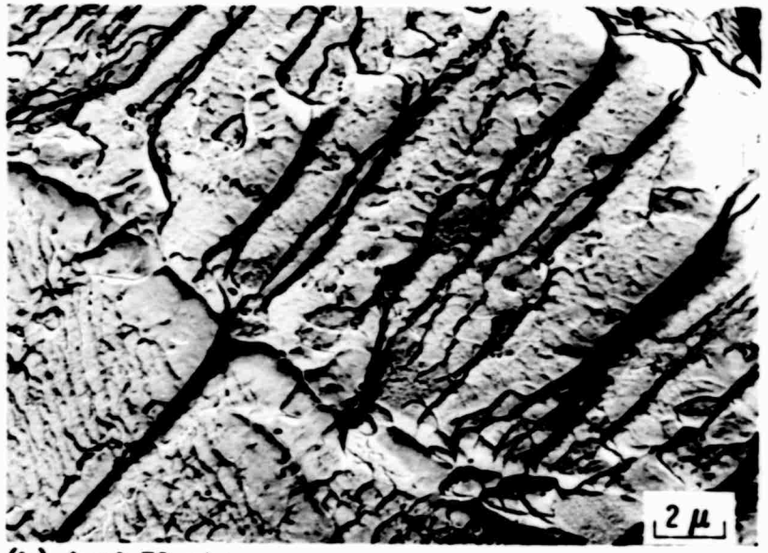

(b) Aged 30 min.

(c) Aged 200 hr.

(d) Aged 200 hr.

Figure 17 Fracture topology of ω-phase-strengthened specimens of Beta III aged at 700°F.

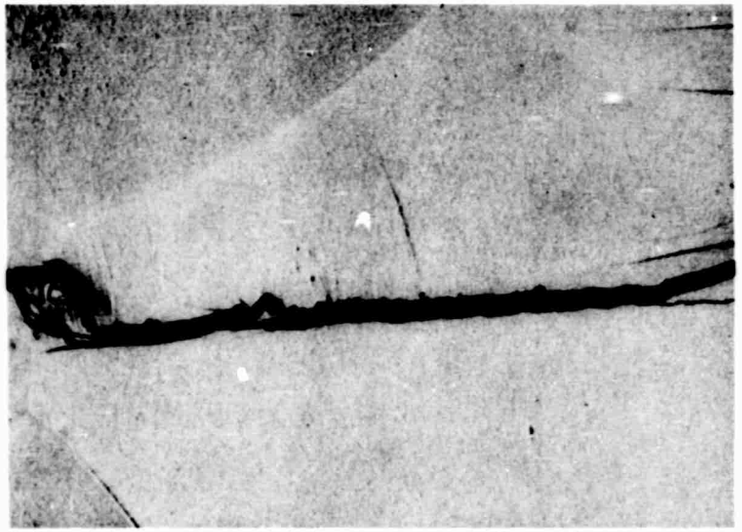

(a) Crack mode 1—cleavage type (X500).

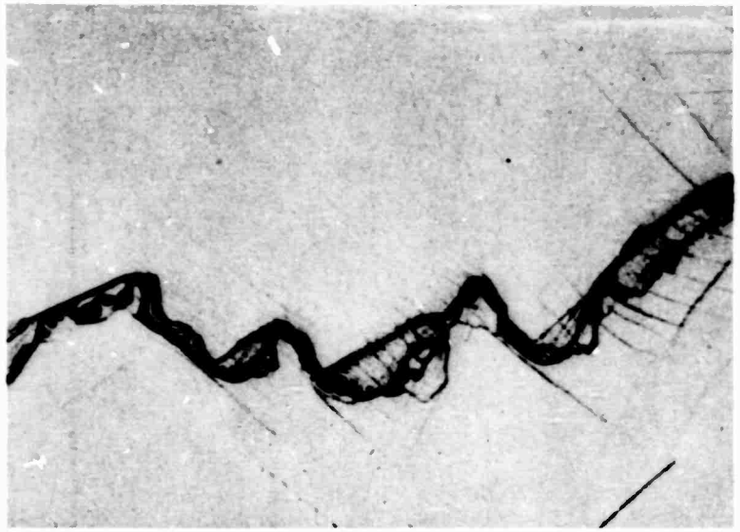

(b) Crack mode 2—discontinuous type (X500).

(c) Slip line morphology—planar slip at A and wavy, branched slip at B (X180).

Figure 18 Crack and slip line morphology in ω-phase-strengthened specimens of Beta III aged 200 hr at 700°F.

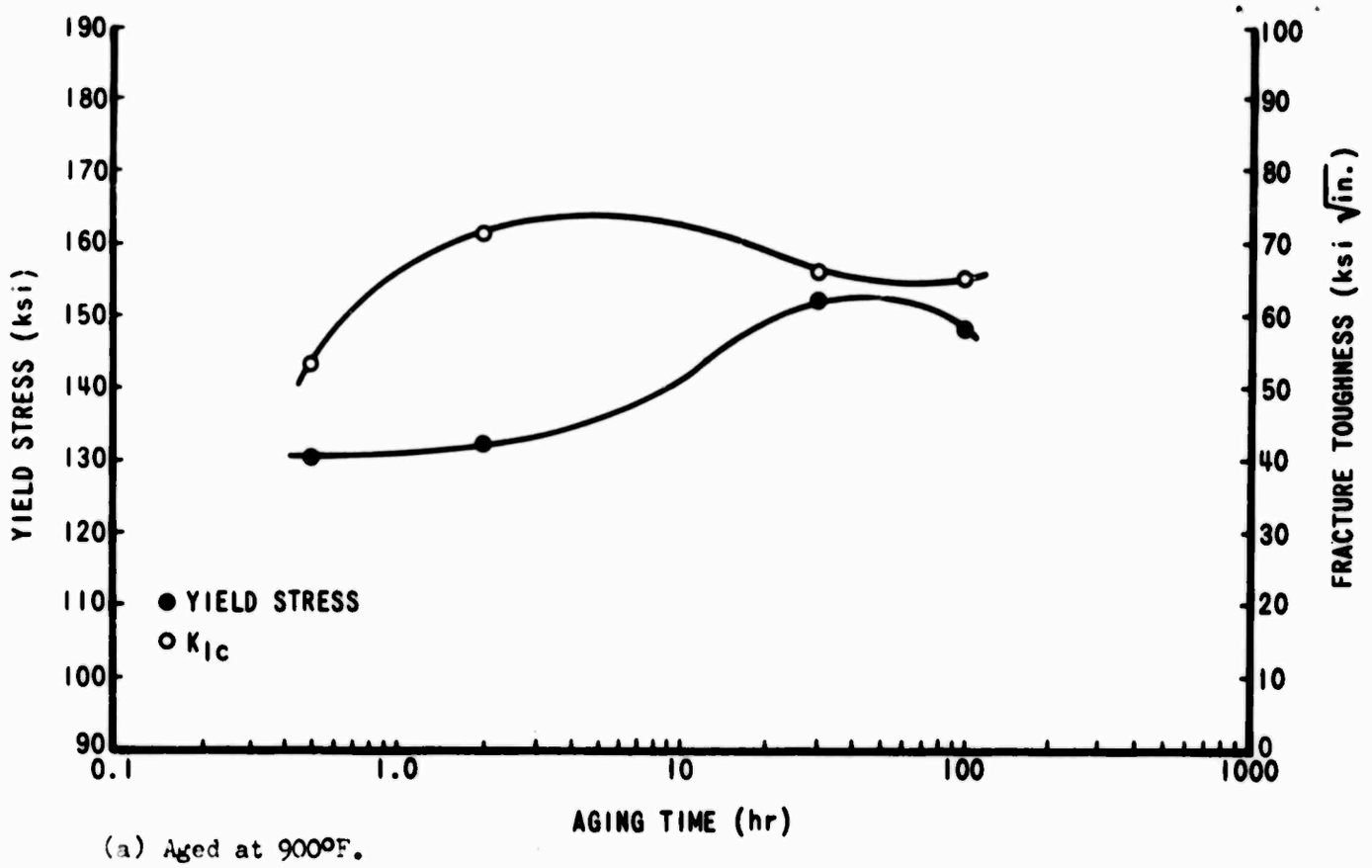

(a) Aged at 900°F.

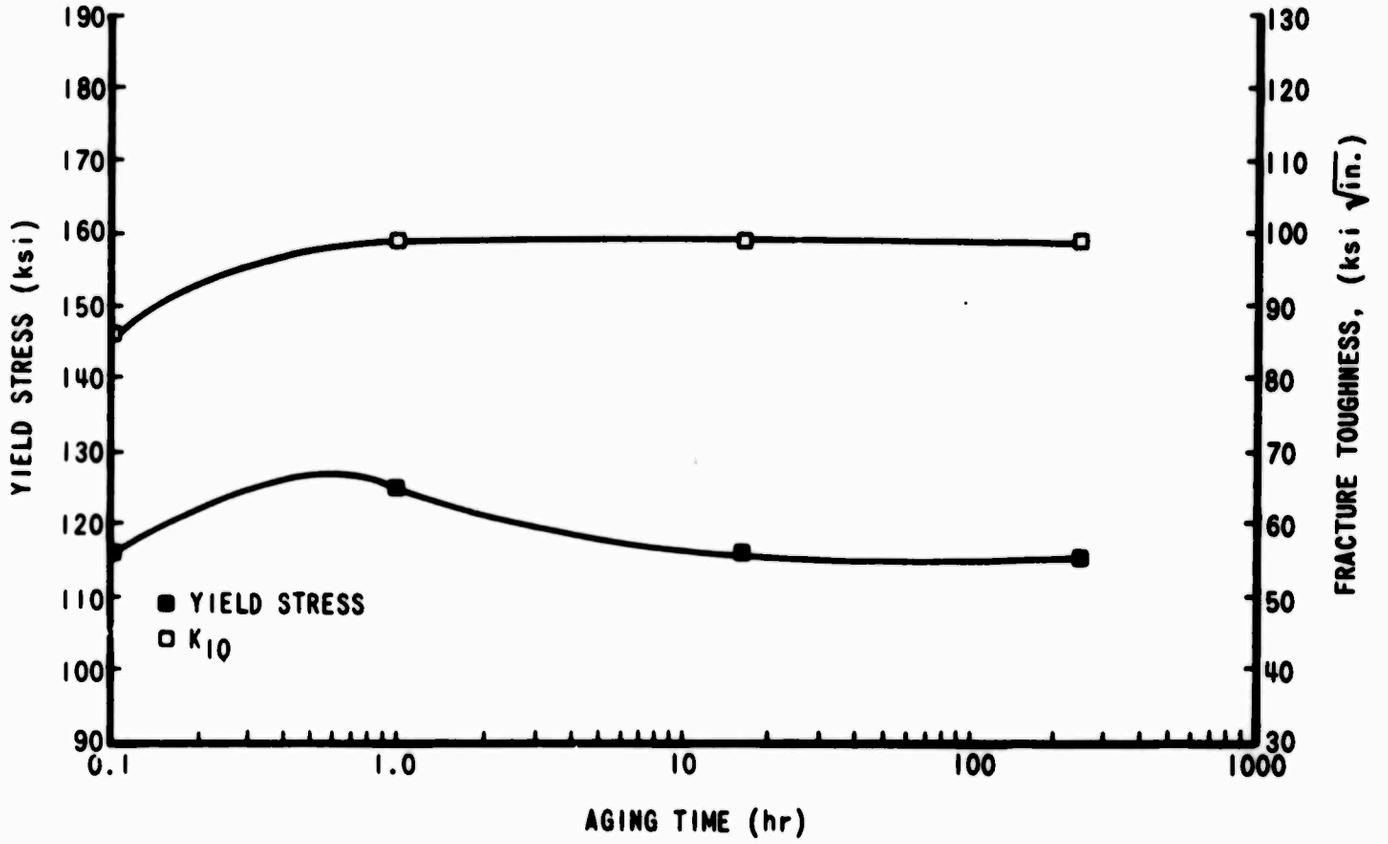

(b) Aged at 1150°F.

Figure 19 Effect of α-phase precipitation on yield strength σ_{ys} and fracture toughness K_{Ic} or K_{IQ} of Beta III.

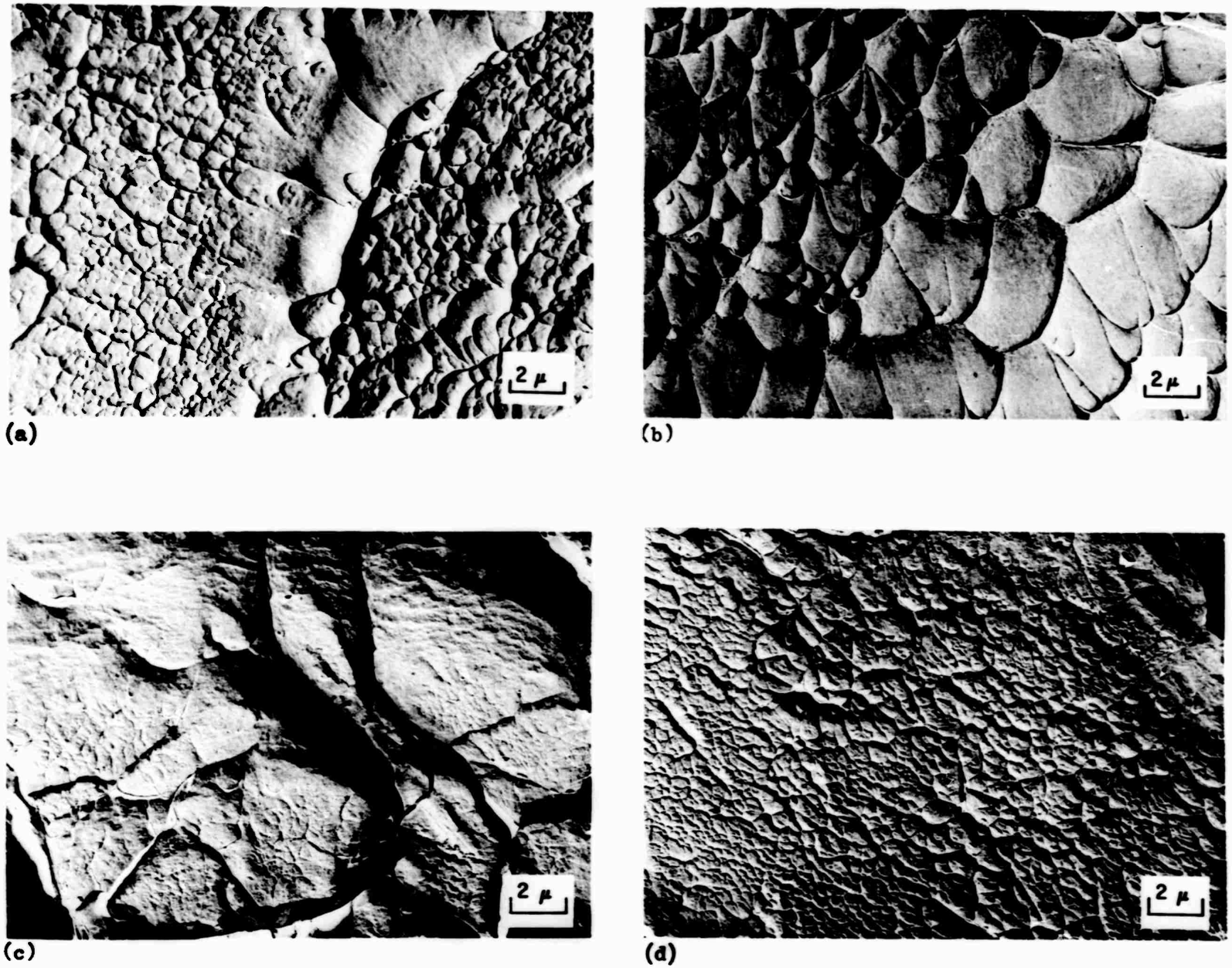

Figure 20 Variation in dimple size in a single specimen of Beta III aged 100 hr at 900°F.

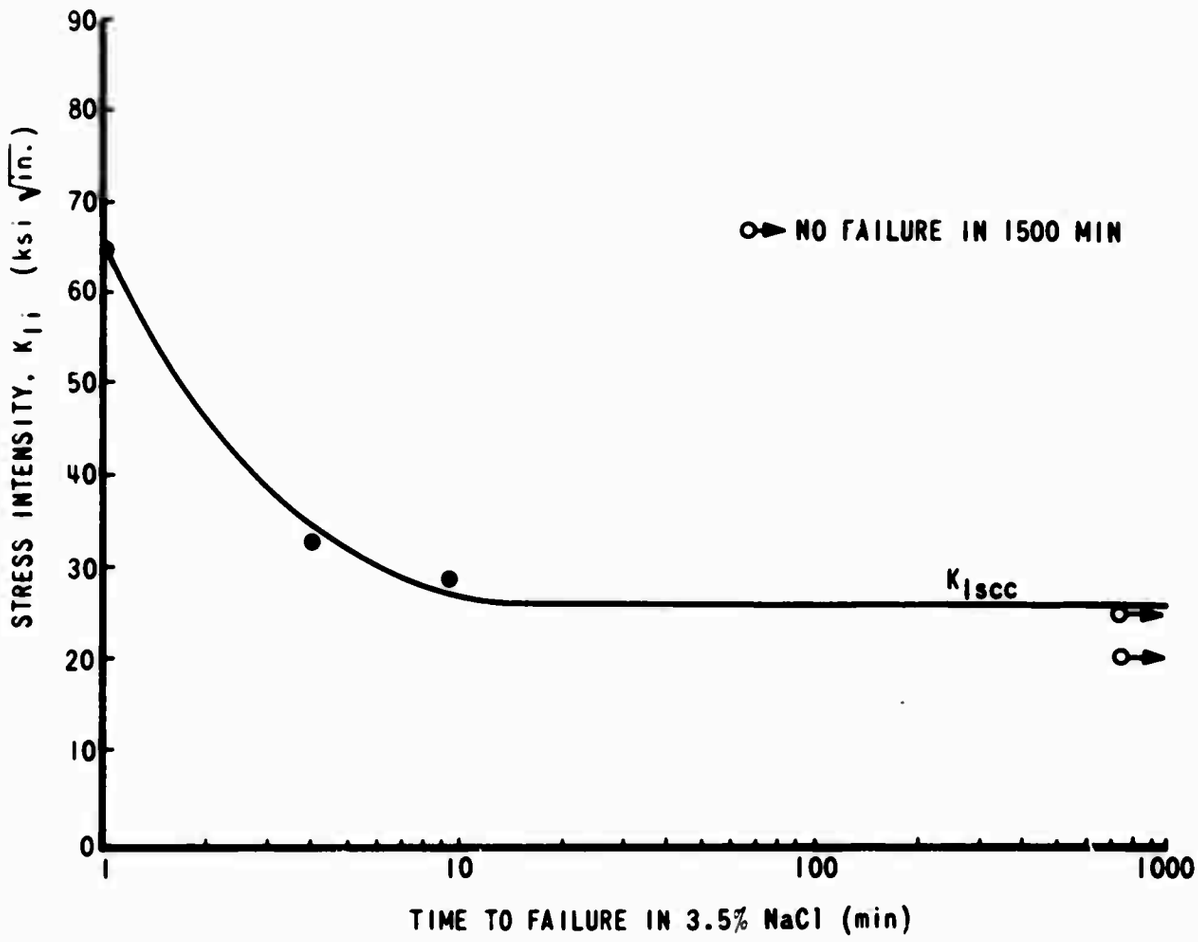

Figure 21 Stress intensity K_{Ii} versus time to failure in 3.5% NaCl solution under open circuit conditions for specimens of Beta III aged 100 hr at 900°F.

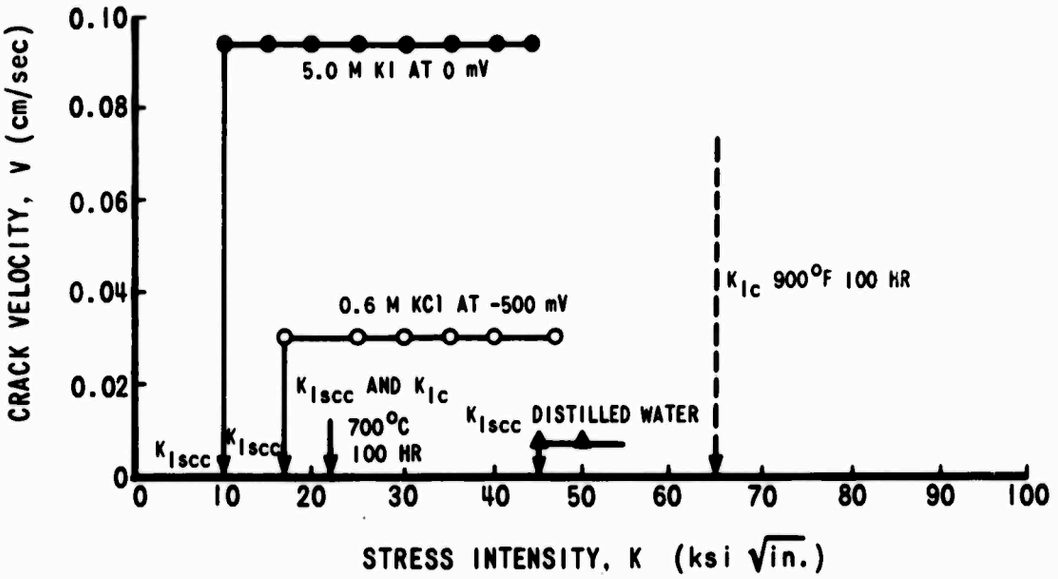

(a) Aged 100 hr at 900°F.

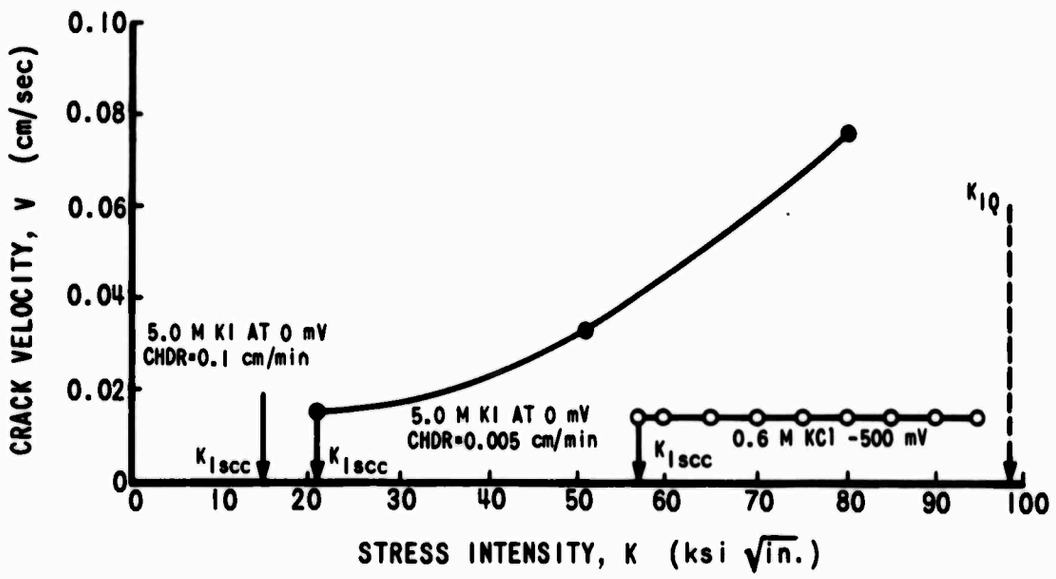

(b) Aged 16 hr at 1150°F.

Figure 22 Variation of crack velocity V with stress intensity K in 0.6 M KCl, 5.0 M KI, and distilled water under controlled potentiostatic conditions. K_{Ic} data are also included.

Figure 23 Optical micrograph showing intergranular stress-corrosion cracking mode in α-phase-strengthened Beta III. Specimen was aged 100 hr at 900°F and tested in 0.6 M KCl (X200).

DOCUMENT CONTROL DATA - R & D

(Security classification of title, body of abstract and indexing annotation must be entered when the overall report is classified)

1 ORIGINATING ACTIVITY (Corporate author)
The Boeing Company
Commercial Airplane Group
Seattle, Washington

2a REPORT SECURITY CLASSIFICATION
Unclassified

2b GROUP

3 REPORT TITLE
Effect of Microstructure on the Strength, Toughness, and Stress-Corrosion Cracking Susceptibility of a Metastable Beta Titanium Alloy (Ti-11.5Mo-6Zr-4.5Sn)

4 DESCRIPTIVE NOTES (Type of report and inclusive dates)
Research Report

5 AUTHOR(S) (Last name, first name, initial)
John A. Feeney
Martin J. Blackburn

6 REPORT DATE	7a TOTAL NO OF PAGES	7b NO OF REFS
February 1970	46	34

8a CONTRACT OR GRANT NO	9a ORIGINATOR'S REPORT NUMBER(S)
N00014-66-C0365 (ARPA Order No. 878)	
b PROJECT NO	
c	9b OTHER REPORT NO(S) (Any other numbers that may be assigned this report)
d.	Boeing Document D6-24472

10 DISTRIBUTION STATEMENT
This document has been approved for public release and sale; its distribution is unlimited.

11 SUPPLEMENTARY NOTES	12 SPONSORING MILITARY ACTIVITY
	Advanced Research Projects Agency, Department of Defense

13 ABSTRACT

This paper describes the influence of microstructure on the mechanical properties of the alloy Ti-11.5Mo-6Zr-4.5Sn. The phase transformations are similar to those that occur in binary Ti-Mo alloys containing 10% to 12% Mo. Thus the β-phase can be retained by quenching from above 1400°F. The β-phase deforms in a complex manner, including mechanical twinning, and is characterized by low strength, high ductility, and high toughness. The ω-phase, which also forms on quenching, is stable at temperatures up to 800°F. Yield strengths of up to 220 ksi have been measured in ($\beta + \omega$) structures, the strength level being dependent on the size and volume fraction of the ω-phase. In contrast, fracture toughness reaches a minimum value of ~ 20 ksi $\sqrt{\text{in.}}$ when the ω-particle size $\geq$ 100 Å. ($\beta + \alpha$) structures show good combinations of yield strength and fracture toughness. Unfortunately, the best combinations are susceptible to stress-corrosion cracking in aqueous solutions containing halide ions.

14 KEY WORDS	LINK A		LINK B		LINK C	
	ROLE	WT	ROLE	WT	ROLE	WT
Metastable Beta Titanium Alloy						
Phase Transformations						
Mechanical Properties						
Fracture Toughness						
Stress Corrosion Cracking						